DESIGNING PRECONDITIONERS FOR SGD: LOCAL CONDITIONING, NOISE FLOORS, AND BASIN STABILITY

MITCHELL SCOTT 1 , TIANSHI XU 1 , ZIYUAN TANG 2 , ALEXANDRA PICHETTE-EMMONS 3 , QIANG YE 3 , YOUSEF SAAD 2 , YUANZHE XI 1

ABSTRACT. Stochastic Gradient Descent (SGD) often slows in the late stage of training due to anisotropic curvature and gradient noise. We analyze preconditioned SGD in the geometry induced by a symmetric positive definite matrix M, deriving bounds in which both the convergence rate and the stochastic noise floor are governed by M-dependent quantities: the rate through an effective condition number in the M-metric, and the floor through the product of that condition number and the preconditioned noise level. For nonconvex objectives, we establish a preconditioner-dependent basin-stability guarantee: when smoothness and basin size are measured in the M-norm, the probability that the iterates remain in a well-behaved local region admits an explicit lower bound. This perspective is particularly relevant in Scientific Machine Learning (SciML), where achieving small training loss under stochastic updates is closely tied to physical fidelity, numerical stability, and constraint satisfaction. The framework applies to both diagonal/adaptive and curvature-aware preconditioners and yields a simple design principle: choose M to improve local conditioning while attenuating noise. Experiments on a quadratic diagnostic and three SciML benchmarks validate the predicted rate—floor behavior.

Introduction

Stochastic Gradient Descent (SGD) has long been the workhorse of large-scale machine learning. Since its early application to multilayer perceptrons in the 1960s[Amari, 1967], its simplicity, scalability, and low per-iteration cost have made it the default optimizer for deep learning models [Bottou et al., 2018]. Classical convergence theory for SGD under noisy gradients typically guarantees a sublinear rate of $\mathcal{O}(1/k)$ under convexity and smoothness assumptions [Robbins and Monro, 1951, Blum, 1954] The theory for SGD convergence under various combinations of conditions is well studied and documented in Garrigos and Gower [2024], Khaled and Richtárik [2023], and Francis Bach [2024]. However, these worst-case bounds often underestimate the actual performance of SGD in practice, particularly during the late stages of training [Bach, 2024].

Recent theoretical developments have established linear convergence for SGD under stronger conditions, such as strong convexity, smoothness, and bounded noise [Bottou et al., 2018]. When the loss F is c-strongly convex, has L-Lipschitz gradients, and the learning rate α satisfies $\alpha \leq \mu/(LK_G)$, the iterates \mathbf{w}_k satisfy

(1)
$$\mathbb{E}[F(\mathbf{w}_k) - F_*] \le (1 - \alpha c\mu)^{k-1} \left(F(\mathbf{w}_1) - F_* - \frac{\alpha LK}{2c\mu} \right) + \frac{\alpha LK}{2c\mu},$$

 $Date \hbox{: November 26, 2025.}$

Corresponding Email: mitchell.scott@emory.edu

MSC2020: Primary 65K10, Secondary 68T05.

¹Department of Mathematics, Emory University, Atlanta, GA,

²Department of Computer Science, University of Minnesota, Minneapolis, MN,

³Department of Mathematics, University of Kentucky, Lexington, KY

where μ , K, and K_G are constants associated with the stochastic gradients (defined in Assumptions 9–11), and $F_* := F(\mathbf{w}^*)$, is the unique minimizer. This bound captures the typical two-phase behavior of convergence: a linear descent phase followed by stagnation at a *noise* floor. Figure 1 illustrates this pattern on a simple MLP trained on Fashion MNIST.

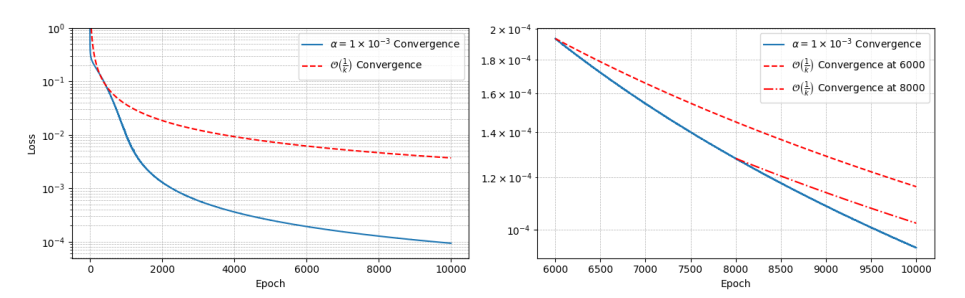


FIGURE 1. Two-layer MLP with 256 hidden units per layer, trained using fixed learning rate SGD (batch size 128) on Fashion MNIST. Left: Theoretical $\mathcal{O}(1/k)$ decay (dashed) versus empirical training loss. Right: Zoom-in on the asymptotic regime showing the noise floor.

The contraction factor $1-\frac{c}{L}\cdot\frac{\mu}{K_G}$ (for $\alpha=\mu/(LK_G)$) and the noise floor $\frac{\alpha LK}{2c\mu}$ in (1) make explicit that late-stage progress is governed by two key factors: conditioning and noise. In Euclidean geometry, the condition number $\kappa=L/c$ is fixed. Introducing a preconditioner—a symmetric positive definite (SPD) matrix M—changes the metric and can simultaneously (i) improve the effective condition number (sharpening the linear contraction) and (ii) lower the noise floor. This motivates a geometry-aware analysis of SGD in which both the rate and the floor are M-dependent quantities.

Main contributions We study how preconditioning affects SGD precisely in the late-stage regime within a well-behaved basin of the loss surface. Rather than proposing a new optimizer, we analyze how applying an SPD matrix \mathbf{M} to rescale the gradient alters both the convergence rate and the noise floor:

- (1) **Strongly convex baseline.** For SGD preconditioned by an SPD matrix **M** and a fixed learning rate, we prove *linear convergence* down to a noise floor. Importantly, the floor scales with the *product* of the effective condition number and the preconditioned noise level. With diminishing learning rates, the floor vanishes and the rate becomes $\mathcal{O}(1/k)$.
- (2) **Local nonconvex regime.** Within a well-behaved basin measured in the M-geometry and a fixed learning rate, we obtain: (i) geometric convergence in expectation down to a noise floor; and (ii) an explicit lower bound on the probability that the iterates remain inside the basin. With harmonic learning rates, the rate is $\mathcal{O}(1/k)$.
- (3) **Design principle and evidence.** Choose **M** to *jointly* improve effective conditioning and reduce the *preconditioned noise level*; the attainable floor moves with their product. The theory covers diagonal/adaptive and curvature-aware preconditioners. Experiments on a quadratic diagnostic and three *Scientific Machine Learning* (SciML) problems corroborate the predicted "faster rate + lower floor" behavior.

While late-stage convergence is broadly relevant, it is especially important in SciML. Here, training losses encode physically meaningful quantities (e.g., PDE residuals, boundary conditions, stability). Unlike standard ML tasks where moderate error may still be acceptable,

small reductions in the final loss can determine whether solutions conserve invariants, remain stable over long horizons, or meet scientific accuracy requirements. In this setting, the optimizer's asymptotic behavior—and particularly the final noise floor—directly governs physical fidelity [Zhang et al., 2024].

Although motivated by SciML, our analysis is general and clarifies why a wide range of methods beyond vanilla SGD perform well in practice. Adaptive algorithms such as Adagrad [Duchi et al., 2011], Adam [Kingma and Ba, 2017], and RMSProp [Hinton, 2014], structured second-order methods such as Shampoo [Gupta et al., 2018], K-FAC [Martens and Grosse, 2015], and Sophia [Liu et al., 2024], as well as quasi-Newton approaches like L-BFGS [Liu and Nocedal, 1989, Chen et al., 2014], can all be viewed through this preconditioning lens: by implicitly or explicitly modifying the local geometry, they improve effective conditioning and/or reduce the gradient noise.

Related work

Recent work has advanced the theoretical understanding of preconditioned and adaptive variants of SGD under various structural and noise assumptions. Koren et al. [2022] showed that preconditioned SGD achieves a rate of $\mathcal{O}(1/\sqrt{k})$ for general stochastic convex optimization, though convergence can stagnate in the presence of persistent gradient noise. Faw et al. [2022] further established that adaptive SGD attains an order-optimal $\tilde{\mathcal{O}}(1/\sqrt{k})$ rate for nonconvex smooth objectives under affine variance conditions, without requiring bounded gradients or finely tuned learning rates. More recently, Attia and Koren [2023] derived high-probability guarantees of $\tilde{\mathcal{O}}(1/k + \sigma_0/\sqrt{k})$ for adaptive methods in both convex and nonconvex settings, relaxing the need for strong smoothness or prior parameter knowledge.

These results primarily address global convergence behavior across general problem classes. In contrast, our analysis focuses on the asymptotic regime—the late stage of training where iterates lie within a well-behaved basin around a local minimizer and optimization progress is limited by curvature anisotropy and gradient noise. In this regime, we show that both the convergence rate and the noise floor of the preconditioned SGD are determined by curvature and variance quantities measured in the preconditioned geometry. This local, geometry-aware viewpoint clarifies why curvature-informed preconditioners and adaptive algorithms yield faster and more stable late-stage convergence.

Other techniques such as batch normalization [Lange et al., 2022] and weight decay [Loshchilov and Hutter, 2017, Barrett and Dherin, 2020] can also be interpreted as implicit forms of preconditioning, though they operate through different regularization mechanisms. For comprehensive surveys of explicit preconditioned SGD and related adaptive methods, we refer the reader to Ye [2024].

Preconditioned SGD convergence analysis

Building on the refined Euclidean analysis of Bottou et al. [2018], we extend the convergence guarantees of SGD to the geometry defined by a preconditioner. In the Euclidean case, the linear convergence rate is governed by the condition number L/c, which determines the contraction factor, while the noise floor in (1) depends on the constant K and scales with KL/c through the admissible learning rate. Preconditioning generalizes this perspective by introducing an SPD matrix M that redefines the geometry of both curvature and noise. The corresponding iteration becomes

(2)
$$\mathbf{w}_{k+1} = \mathbf{w}_k - \alpha_k \mathbf{M}^{-1} g(\mathbf{w}_k, \boldsymbol{\xi}_k),$$

where $g(\mathbf{w}_k, \boldsymbol{\xi}_k) = \nabla_w F_k(\mathbf{w})$ is the stochastic gradient, α_k is the learning rate, $\boldsymbol{\xi}_k$ is an i.i.d. sample drawn at iteration k, and \mathbf{M} is the preconditioner. The standard (vanilla) SGD update is recovered when $\mathbf{M} = \mathbf{I}$.

We first analyze the globally strongly convex case as a baseline to make the role of the preconditioned geometry explicit. Although this setting is rarely realized in deep learning, it reveals the essential mechanism through which preconditioning affects convergence. The analysis shows how curvature and noise floor transform under a change of metric, providing a principled way to compare different choices of \mathbf{M} . This also lays the groundwork for the local nonconvex analysis in Section , where \mathbf{M} influences both basin size and stability.

Convergence in the globally strongly convex setting We establish convergence guarantees for preconditioned SGD when the objective is globally strongly convex. This simplified setting allows for a transparent analysis of how a preconditioner reshapes both the effective curvature (governing contraction rate) and the gradient noise (governing the asymptotic error). While the derivations parallel the Euclidean case, expressing them in the M-induced geometry makes the dependence on the preconditioner explicit and lays the groundwork for the more general nonconvex results to follow.

Curvature assumptions. Preconditioning redefines smoothness and strong convexity through effective constants (\hat{L}, \hat{c}) measured in the **M**-induced norm.

Assumption 1 (M-strong convexity). $F: \mathbb{R}^d \to \mathbb{R}$ is M-strongly convex: there exists $\hat{c} > 0$ such that

$$F(\overline{\mathbf{w}}) \ge F(\mathbf{w}) + \nabla F(\mathbf{w})^{\top} (\overline{\mathbf{w}} - \mathbf{w}) + \frac{1}{2} \hat{c} \|\overline{\mathbf{w}} - \mathbf{w}\|_{\mathbf{M}}^{2}, \quad \forall \overline{\mathbf{w}}, \mathbf{w} \in \mathbb{R}^{d}.$$

Assumption 2 (M-Lipschitz gradient). ∇F is M-Lipschitz with constant $\hat{L} > 0$:

$$\|\nabla F(\overline{\mathbf{w}}) - \nabla F(\mathbf{w})\|_{\mathbf{M}^{-1}} \leq \hat{L} \|\overline{\mathbf{w}} - \mathbf{w}\|_{\mathbf{M}}, \quad \forall \, \overline{\mathbf{w}}, \mathbf{w} \in \mathbb{R}^d.$$

These conditions are direct analogues of the Euclidean definitions. Writing $\mathbf{M}^{-1} = \mathbf{P}\mathbf{P}^{\top}$ gives the spectral characterization:

Lemma 1. Let F be twice differentiable and $\mathbf{M}^{-1} = \mathbf{P}\mathbf{P}^{\top}$. Then: (i) ∇F is \mathbf{M} -Lipschitz with constant $\hat{L} \iff$ all eigenvalues of $\mathbf{P}^{\top}\nabla^{2}F(\mathbf{w})\mathbf{P}$ are $\leq \hat{L}$; (ii) F is \mathbf{M} -strongly convex with constant $\hat{c} \iff$ all eigenvalues of $\mathbf{P}^{\top}\nabla^{2}F(\mathbf{w})\mathbf{P}$ are $\geq \hat{c}$.

Hence preconditioning improves the effective condition number whenever $\hat{L}/\hat{c} < L/c$. Noise assumptions. We measure the first and second moments of the stochastic gradient in the \mathbf{M}^{-1} -norm. Define the conditional variance

(3)
$$\mathbb{V}_{\boldsymbol{\xi}_k} [g(\mathbf{w}_k, \boldsymbol{\xi}_k), \| \cdot \|_{\mathbf{M}^{-1}}] := \mathbb{E}_{\boldsymbol{\xi}_k} [\|g(\mathbf{w}_k, \boldsymbol{\xi}_k)\|_{\mathbf{M}^{-1}}^2] - \|\mathbb{E}_{\boldsymbol{\xi}_k} [g(\mathbf{w}_k, \boldsymbol{\xi}_k)]\|_{\mathbf{M}^{-1}}^2.$$

Assumption 3 (Moment bounds in \mathbf{M}^{-1}). For the iterates of (2), there exist constants $\mu_G \ge \mu > 0$, $K \ge 0$, and $K_V \ge 0$ such that, for all k,

(4)
$$\langle \nabla F(\mathbf{w}_k), \mathbb{E}_{\boldsymbol{\xi}_{\ell}}[g(\mathbf{w}_k, \boldsymbol{\xi}_k)] \rangle_{\mathbf{M}^{-1}} \ge \mu \|\nabla F(\mathbf{w}_k)\|_{\mathbf{M}^{-1}}^2,$$

(5)
$$\|\mathbb{E}_{\boldsymbol{\xi}_{k}}[g(\mathbf{w}_{k}, \boldsymbol{\xi}_{k})]\|_{\mathbf{M}^{-1}} \leq \mu_{G} \|\nabla F(\mathbf{w}_{k})\|_{\mathbf{M}^{-1}},$$

(6)
$$\mathbb{V}_{\boldsymbol{\xi}_k}[g(\mathbf{w}_k, \boldsymbol{\xi}_k), \|\cdot\|_{\mathbf{M}^{-1}}] \leq K + K_V \|\nabla F(\mathbf{w}_k)\|_{\mathbf{M}^{-1}}^2.$$

We call K the preconditioned noise level because the variance in the \mathbf{M}^{-1} -norm satisfies

$$\mathbb{V}_{\boldsymbol{\xi}}\big[g(\mathbf{w},\boldsymbol{\xi}),\|\cdot\|_{\mathbf{M}^{-1}}\big] \ = \ \mathrm{tr}\big(\mathbf{M}^{-1}\boldsymbol{\Sigma}(\mathbf{w})\big),$$

where $\Sigma(\mathbf{w}) := \operatorname{Cov}(g(\mathbf{w}, \boldsymbol{\xi}) \mid \mathbf{w})$. In the stationary case $\Sigma(\mathbf{w}) \equiv \Sigma$, we have the fixed $\operatorname{tr}(\mathbf{M}^{-1}\Sigma)$. More generally, on a region containing the iterates it is natural to choose $K \geq \sup_{\mathbf{w}} \operatorname{tr}(\mathbf{M}^{-1}\Sigma(\mathbf{w}))$, so K is a uniform baseline for the preconditioned noise.

Under these assumptions we obtain the usual linear and sublinear rates, but with constants that depend explicitly on the preconditioned geometry.

Theorem 2. Under Assumptions 1–3 (with $F_{\min} = F_*$), suppose (2) uses a fixed learning rate $\alpha_k = \overline{\alpha}$ with

$$0 < \overline{\alpha} \le \frac{\mu}{\hat{L} K_G}$$
 where $K_G = K_V + \mu_G^2 \ge \mu^2 > 0$.

Then, for all $k \in \mathbb{N}$,

$$(7) \quad \mathbb{E}[F(\mathbf{w}_k) - F_*] \leq \frac{\overline{\alpha} \,\hat{L} \,K}{2 \,\hat{c} \,\mu} + (1 - \overline{\alpha} \,\hat{c} \,\mu)^{k-1} \left(F(\mathbf{w}_1) - F_* - \frac{\overline{\alpha} \,\hat{L} \,K}{2 \,\hat{c} \,\mu} \right) \xrightarrow{k \to \infty} \frac{\overline{\alpha} \,\hat{L} \,K}{2 \,\hat{c} \,\mu}.$$

Theorem 2 shows that, with a fixed learning rate $\overline{\alpha}$, preconditioned SGD contracts linearly with factor $1 - \overline{\alpha} \hat{c} \mu$ and converges to an asymptotic floor

$$\frac{\overline{\alpha}\,\hat{L}\,K}{2\,\hat{c}\,\mu} = \frac{\overline{\alpha}}{2\mu} \left(\frac{\hat{L}}{\hat{c}}\right) K.$$

Thus, the floor factorizes into an effective condition number \hat{L}/\hat{c} and a preconditioned noise level K. In the late stage of training, we have $F(\mathbf{w}_k) - F_* = \mathcal{O}(\overline{\alpha}K)$ and $\|\nabla F(\mathbf{w}_k)\|_{\mathbf{M}^{-1}}^2 = \mathcal{O}(\overline{\alpha}K)$. Substituting into the variance bound (6) gives

$$\mathbb{V}_{\boldsymbol{\xi}_k}[g(\mathbf{w}_k, \boldsymbol{\xi}_k), \|\cdot\|_{\mathbf{M}^{-1}}] \leq K + \mathcal{O}(\overline{\alpha}K),$$

so for small $\overline{\alpha}$ the variance is dominated by the baseline K term.

Moreover, since $\mathbb{V}_{\boldsymbol{\xi}}[g(\mathbf{w},\boldsymbol{\xi}),\|\cdot\|_{\mathbf{M}^{-1}}] = \operatorname{tr}(\mathbf{M}^{-1}\boldsymbol{\Sigma}(\mathbf{w}))$, we may view K as an upper baseline for the preconditioned noise $\operatorname{tr}(\mathbf{M}^{-1}\boldsymbol{\Sigma}(\mathbf{w}))$ along the late–stage trajectory. Preconditioning reduces this baseline through its effect on $\operatorname{tr}(\mathbf{M}^{-1}\boldsymbol{\Sigma}(\mathbf{w}))$; choosing \mathbf{M} to attenuate high–variance directions lowers this trace and thus lowers the effective noise floor.

Theorem 3. Under Assumptions 1–3 (with $F_{\min} = F_*$), suppose (2) uses $\alpha_k = \beta/(\gamma + k)$ with $\beta > \frac{1}{\hat{c}\,\mu}$ and $\gamma > 0$ chosen so that $\alpha_1 \leq \mu/(\hat{L}K_G)$. Then, for all $k \in \mathbb{N}$,

(8)
$$\mathbb{E}[F(\mathbf{w}_k) - F_*] \leq \frac{\nu}{\gamma + k}, \qquad \nu := \max \left\{ \frac{\beta^2 \hat{L}K}{2(\beta \hat{c}\mu - 1)}, (\gamma + 1) \left(F(\mathbf{w}_1) - F_* \right) \right\}.$$

With diminishing learning rates, the noise floor vanishes and Theorem 3 shows that preconditioned SGD attains the optimal $\mathcal{O}(1/k)$ rate. Preconditioning no longer changes the rate itself—it always decays like 1/k—but it directly influences the leading constant ν which has the same structure as the fixed-learning-rate floor: an effective condition number \hat{L}/\hat{c} multiplied by the preconditioned noise level K. Thus even when the noise floor disappears, late–stage performance is still governed by the same metric–dependent quantities (\hat{L}, \hat{c}, K) . Consequently, effective preconditioners must again balance curvature alignment (to reduce \hat{L}/\hat{c}) with noise attenuation (to reduce K), improving both the asymptotic constants in the $\mathcal{O}(1/k)$ regime. Local convergence in the nonconvex setting The empirical loss $F(\mathbf{w})$ over network parameters is typically nonconvex, and its local geometry near minimizers is rarely strictly convex. Empirical studies show that trained models often converge to regions that are flat in many directions and exhibit highly degenerate curvature—manifested as a cluster of very small or near-zero eigenvalues in the Hessian—arising from overparameterization, symmetries, and parameter non-identifiability [Sagun et al., 2018, Ghorbani et al., 2019]. Despite this degeneracy, the optimization dynamics remain structured: iterates contract along directions with significant curvature while the loss changes little along flat directions. To describe this late-stage regime without assuming strong convexity, we impose a local Polyak–Lojasiewicz (PL) condition [Chan, 1979, Karimi et al., 2016] in the M–geometry, which enforces gradient domination only in informative directions and tolerates flat or weakly curved subspaces. This flat-tolerant formulation provides a natural framework to study how preconditioning reshapes local curvature and noise, governing contraction rates, asymptotic error floors, and stability during the final phase of optimization.

Additional local assumptions. Fix an SPD matrix \mathbf{M} and an open neighborhood $\mathcal{U} \subset \mathbb{R}^d$. Assume the local minimizer set

$$\mathcal{S} := \arg\min_{\mathbf{w} \in \mathcal{U}} F(\mathbf{w}) \neq \varnothing, \qquad F_* := \min_{\mathbf{w} \in \mathcal{U}} F(\mathbf{w}) = F(\mathbf{s}) \text{ for any } \mathbf{s} \in \mathcal{S}.$$

Write $||x||_{\mathbf{M}} := (x^{\top} \mathbf{M} x)^{1/2}$ and $\operatorname{dist}_{\mathbf{M}}(\mathbf{w}, \mathcal{S}) := \inf_{\mathbf{s} \in \mathcal{S}} ||\mathbf{w} - \mathbf{s}||_{\mathbf{M}}$. For radii $0 < r < r_+$, define the \mathbf{M} -metric neighborhoods

$$\mathcal{N}_r := \{ \mathbf{w} : \operatorname{dist}_{\mathbf{M}}(\mathbf{w}, \mathcal{S}) \le r \}, \qquad \mathcal{N}_{r_{\perp}} := \{ \mathbf{w} : \operatorname{dist}_{\mathbf{M}}(\mathbf{w}, \mathcal{S}) \le r_{\perp} \} \subseteq \mathcal{U}.$$

We assume the following conditions hold on \mathcal{N}_r (for the iterates) and on \mathcal{N}_{r_+} (for the exit bound).

Assumption 4 (Local M–PL on \mathcal{N}_r). There exists $\hat{\mu}_{PL} > 0$ such that, for all $\mathbf{w} \in \mathcal{N}_r$,

$$2\hat{\mu}_{\mathrm{PL}}(F(\mathbf{w}) - F_*) < \|\nabla F(\mathbf{w})\|_{\mathbf{M}^{-1}}^2.$$

Assumption 5 (Local M–Lipschitz gradient on a convex neighborhood of \mathcal{N}_{r_+}). There exists an open convex set \mathcal{V} with $\mathcal{N}_{r_+} \subset \mathcal{V} \subseteq \mathcal{U}$ and a constant $\hat{L} > 0$ such that, for all $\overline{\mathbf{w}}, \mathbf{w} \in \mathcal{V}$,

$$\|\nabla F(\overline{\mathbf{w}}) - \nabla F(\mathbf{w})\|_{\mathbf{M}^{-1}} \leq \hat{L} \|\overline{\mathbf{w}} - \mathbf{w}\|_{\mathbf{M}}.$$

Assumption 6 (Local stochastic gradient conditions on \mathcal{N}_r). Let (\mathcal{F}_k) denote the natural filtration and set $g_k := g(\mathbf{w}_k, \boldsymbol{\xi}_k)$. There exist constants $\mu \in (0, 1]$, $K_G \geq 0$, and $K \geq 0$ such that, for every k with $\mathbf{w}_k \in \mathcal{N}_r$,

$$\langle \nabla F(\mathbf{w}_k), \mathbb{E}[g_k \mid \mathcal{F}_k] \rangle_{\mathbf{M}^{-1}} \geq \mu \|\nabla F(\mathbf{w}_k)\|_{\mathbf{M}^{-1}}^2, \qquad \mathbb{E}[\|g_k\|_{\mathbf{M}^{-1}}^2 \mid \mathcal{F}_k] \leq K_G \|\nabla F(\mathbf{w}_k)\|_{\mathbf{M}^{-1}}^2 + K.$$

Assumption 7 (Local quadratic growth (QG) on \mathcal{N}_{r_+}). There exists $\alpha_{\text{QG}} > 0$ such that, for all $\mathbf{w} \in \mathcal{N}_{r_+}$,

$$F(\mathbf{w}) - F_* \geq \frac{\alpha_{\text{QG}}}{2} \operatorname{dist}_{\mathbf{M}}(\mathbf{w}, \mathcal{S})^2.$$

Assumption 8 (One-step containment). If $\mathbf{w}_k \in \mathcal{N}_r$, then $\mathbf{w}_{k+1} \in \mathcal{N}_{r_+}$ almost surely.

These local assumptions are the basin–restricted analogue of the global conditions in Section . The local \mathbf{M} –PL condition replaces global strong convexity by a $\operatorname{gradient-domination}$ inequality in the \mathbf{M} –metric, enforcing curvature only in directions that matter while allowing flat or weakly curved directions—precisely the situation observed near low-loss regions of overparameterized

models [Sagun et al., 2018, Ghorbani et al., 2019]. The local M-Lipschitz condition on a convex neighborhood $V \supset \mathcal{N}_{r_+}$ guarantees the quadratic upper bound

$$F(\overline{\mathbf{w}}) \leq F(\mathbf{w}) + \nabla F(\mathbf{w})^{\top} (\overline{\mathbf{w}} - \mathbf{w}) + \frac{\hat{L}}{2} \|\overline{\mathbf{w}} - \mathbf{w}\|_{\mathbf{M}}^{2}$$

for every update step that remains in the basin \mathcal{N}_{r_+} . The one-step containment assumption ensures that, for sufficiently small learning rates, the iterates never leave this well-behaved region, so all local bounds remain valid along the trajectory. The local stochastic condition (Assumption 6) matches the structure of the global moment bounds in Assumption 3, but only needs to hold for $\mathbf{w}_k \in \mathcal{N}_r$. Finally, the local QG condition ensures that the objective value increases at least quadratically with $\mathrm{dist}_{\mathbf{M}}(\mathbf{w}, \mathcal{S})$ near the basin boundary—a property that holds when the Hessian is positive definite in normal directions and that supports the optional-stopping argument used in the exit-probability analysis. Collectively, these assumptions describe a local regime that accommodates moderate nonconvexity and flatness while still providing sufficient structure for quantitative convergence analysis.

Theorem 4 (Convergence to a local minimizer). Assume Assumptions 4 and 6 on \mathcal{N}_r , Assumption 5 on a convex set \mathcal{V} with $\mathcal{N}_{r_+} \subset \mathcal{V} \subseteq \mathcal{U}$, Assumption 7 on \mathcal{N}_{r_+} for some $r_+ > r$, and Assumption 8. Let $\tau := \inf\{k \geq 1 : \mathbf{w}_k \notin \mathcal{N}_r\}$ and suppose $\mathbf{w}_1 \in \mathcal{N}_r$. Fix any constant learning rate $\overline{\alpha}$ satisfying

$$0 < \overline{\alpha} < \min \left\{ \frac{\mu}{\hat{L} K_G} \,, \, \frac{\alpha_{\rm QG} \, \hat{\mu}_{\rm PL} \, \mu}{\hat{L} \, K} \, r^2 \,, \, \frac{1}{\mu \, \hat{\mu}_{\rm PL}} \right\},$$

and define

$$\rho := \overline{\alpha} \, \hat{\mu}_{\mathrm{PL}} \, \mu \in (0, 1), \qquad C := \frac{\overline{\alpha} \, \hat{L} \, K}{2 \, \hat{\mu}_{\mathrm{PL}} \, \mu}.$$

Then, on the event $\{\tau = \infty\}$, the iterates exhibit conditional geometric convergence in expectation to the noise floor C: for all $k \geq 1$,

$$\mathbb{E}[F(\mathbf{w}_k) - F_* \mid \tau = \infty] \le C + (1 - \rho)^{k-1} (F(\mathbf{w}_1) - F_* - C),$$

and in particular $\mathbb{E}[F(\mathbf{w}_k) - F_* \mid \tau = \infty] \to C$ as $k \to \infty$. Moreover, the exit time τ satisfies the basin-stability bound

$$\mathbb{P}(\tau = \infty) \geq \max \left\{ 0, \ 1 - \frac{F(\mathbf{w}_1) - F_*}{\frac{\alpha_{QG}}{2} \ r^2} \right\}.$$

Under local PL, the fixed learning rate floor is again a product of local effective conditioning $(\hat{L}/\hat{\mu}_{\text{PL}})$ and the preconditioned noise level K.

Theorem 5 (Diminishing learning rate, local regime). Assume Assumptions 4 and 6 hold on \mathcal{N}_r , Assumption 5 holds on a convex \mathcal{V} with $\mathcal{N}_{r_+} \subset \mathcal{V} \subseteq \mathcal{U}$, Assumption 7 holds on \mathcal{N}_{r_+} for some $r_+ > r$, and Assumption 8 holds. Let $\tau := \inf\{k \geq 1 : \mathbf{w}_k \notin \mathcal{N}_r\}$ and $\mathbf{w}_1 \in \mathcal{N}_r$. Consider harmonic learning rates

$$\alpha_k = \frac{\beta}{\gamma + k}, \quad \gamma > 0, \quad \frac{2}{\hat{\mu}_{\rm PL} \, \mu} < \beta \le \frac{\mu(\gamma + 1)}{\hat{L} \, K_G},$$

and define

$$\nu \ := \ \max \left\{ \frac{\beta^2 \hat{L} K}{2 \left(\beta \hat{\mu}_{\mathrm{PL}} \mu - 1\right)}, \ (\gamma + 1) \left[F(\mathbf{w}_1) - F_* \right] \right\}.$$

Then

$$\mathbb{P}(\tau = \infty) \geq \max \left\{ 0, \ 1 - \frac{F(\mathbf{w}_1) - F_*}{\frac{\alpha_{\text{QG}}}{2} \ r^2} \right\},\,$$

and, on the event $\{\tau = \infty\}$, we have the conditional rate

$$\mathbb{E}[F(\mathbf{w}_k) - F_* \mid \tau = \infty] \leq \frac{\nu}{\gamma + k} \qquad \forall k \geq 1.$$

Theorem 4 (fixed learning rates) and Theorem 5 (diminishing learning rates) show that once the iterates enter a local basin, optimization exhibits geometric or $\mathcal{O}(1/k)$ convergence with constants determined by the local PL constant $\hat{\mu}_{\text{PL}}$, local Lipschitz constant \hat{L} and the preconditioned noise level K. In contrast to the globally strongly convex case, these constants depend only on the geometry of the basin actually explored by the iterates. Stability is governed separately by the local QG constant α_{QG} and the radius r through the product $\alpha_{\text{QG}}r^2$, which controls the probability of remaining in the basin.

The local PL and QG conditions capture different geometric aspects: $\hat{\mu}_{PL}$ quantifies gradient domination, while α_{QG} measures how the objective grows with distance from the minimizer set \mathcal{S} . They need not be related in general nonconvex settings. In a locally quadratic regime they become comparable, as both are controlled by the smallest normal curvature in the M–geometry. This highlights a key distinction from the global strongly convex case: locally, convergence and stability are driven by curvature in the normal directions to \mathcal{S} , whereas flat or weakly curved tangential directions are allowed.

Because all constants in the local bounds depend on the M-metric, a well-designed preconditioner M can improve late-stage behavior by (i) enhancing local conditioning—decreasing $\hat{L}/\hat{\mu}_{\rm PL}$ and thereby speeding up contraction; (ii) reducing the preconditioned noise level K, lowering the effective noise floor; and (iii) when aligned with normal-space curvature, increasing $\alpha_{\rm QG}$ and, in some cases, permitting a larger certifiable radius r, which jointly improves basin stability.

Practical preconditioners for SGD A wide range of preconditioning strategies are used in modern machine learning. On the first-order side, adaptive methods such as Adam [Kingma and Ba, 2017], AMSGrad [Reddi et al., 2018], PAdam [Chen et al., 2020], and Yogi [Zaheer et al., 2018] implicitly apply diagonal preconditioners by rescaling gradients with running estimates of coordinatewise second moments. On the second-order side, curvature-aware preconditioners exploit Hessian or Fisher Information Matrix (FIM) structure, including the empirical FIM [Schraudolph, 2002], full or mini-batch Hessians [Fletcher, 2013, Garg et al., 2024], mini-batch quasi-Newton updates [Griffin et al., 2022], and Kronecker-factored FIM (K-FAC) [Martens and Grosse, 2015]. Classical schemes such as L-BFGS [Liu and Nocedal, 1989, Chen et al., 2014] can also be viewed as low-rank, history-based preconditioners. Appendix summarizes these approaches and their computational trade-offs.

The convergence analysis in Sections – suggests two practical mechanisms through which preconditioners shape late-stage behavior:

- Local conditioning. Curvature-aware preconditioners (e.g., Fisher, Gauss-Newton, Hessian, K-FAC) tend to reduce the metric-smoothness constant \hat{L} and can increase the local PL constant $\hat{\mu}_{PL}$. In our bounds, this improves the effective local condition number $\hat{L}/\hat{\mu}_{PL}$, permits larger admissible fixed learning rates $\alpha \leq \mu/(\hat{L}K_G)$, and reduces the leading constant under diminishing learning rates.
- \bullet Noise attenuation. Preconditioners aligned with the gradient-noise structure reduce the preconditioned noise level K in the late-stage regime. Together with improved

conditioning (smaller \hat{L}/\hat{c} or $\hat{L}/\hat{\mu}_{\rm PL}$), this lowers the noise floor, which scales with their *product*. Fisher-based and related methods are especially effective because they explicitly incorporate gradient statistics.

These two mechanisms—improved conditioning and reduced preconditioned noise—match the behavior observed in Section . Curvature-matched preconditioners (Fisher, Gauss–Newton, K-FAC, Hessian) typically yield faster late-stage contraction by reducing \hat{L} and, in some cases, increasing $\hat{\mu}_{PL}$, while their use of gradient second-moment information tends to reduce K. Adaptive/diagonal methods likewise lower K by damping high-variance coordinates, though their alignment with curvature is typically weaker.

Numerical results

Many machine-learning benchmarks illustrate the benefits of preconditioned SGD (e.g., Schmidt et al. [2021], Schneider et al. [2019]), but our emphasis is on SciML, where driving the loss to very small values is tightly linked to physical fidelity, numerical stability, and constraint satisfaction [Kaplan et al., 2020, Swersky et al., 2011]. We therefore structure the experiments in two parts.

First, we analyze a diagnostic quadratic model in which all the quantities in our theory— \hat{L} , $\hat{\mu}_{\text{PL}}$, and the preconditioned noise level K—admit closed forms. This allows us to directly compute the geometry— and noise–dependent metrics from Sections – and verify their influence on rate and floor.

Second, we examine three representative SciML problems: noisy Franke surface regression [Franke, 1979], a Poisson-type PINN, and Green's-function learning for diffusion and convection-diffusion [Zhang et al., 2024, Rathore et al., 2024, Hao et al., 2024, Xu et al., 2025], to see how the theoretical mechanisms are reflected in practical settings.

Diagnostic quadratic model To isolate the effects predicted by the theory, we consider the quadratic objective

$$F(\mathbf{w}) = \frac{1}{2} (\mathbf{w} - \mathbf{w}^*)^{\top} \mathbf{H} (\mathbf{w} - \mathbf{w}^*) + F_*, \qquad \mathbf{H} \succeq 0,$$

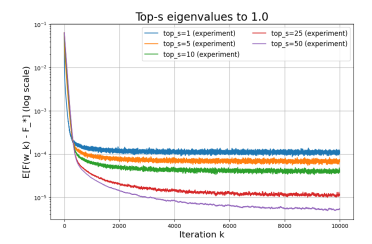
here **H** specifies curvature. We test two simple, analytically tractable choices: Euclidean SGD $(\mathbf{M} = \mathbf{I})$ and a low-rank curvature-aware preconditioner $\mathbf{M} = \mathbf{I} + \mathbf{U}_s(\widetilde{\mathbf{\Lambda}}_s - \mathbf{I})\mathbf{U}_s^{\top}$, where \mathbf{U}_s contains the top (or bottom) s eigenvectors of **H** and $\widetilde{\mathbf{\Lambda}}_s$ is a diagonal matrix. This model captures the essential effect of curvature information. We used a fixed learning rate.

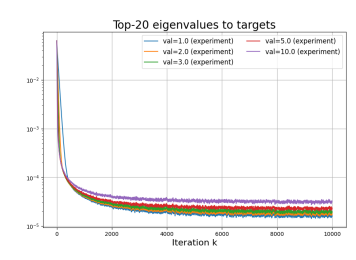
Instead of forming a dataset, we synthesize unbiased mini-batch gradients

$$g_k = \nabla F(\mathbf{w}_k) + \zeta_k, \qquad \mathbb{E}[\zeta_k] = 0, \quad \text{Cov}(\zeta_k) = \frac{1}{B} \Sigma.$$

To match the second-order statistics of least-squares problems near \mathbf{w}^* , we set $\mathbf{\Sigma} = \sigma^2 \mathbf{H}$, giving $K = \frac{\sigma^2}{B} \operatorname{tr}(\mathbf{M}^{-1}\mathbf{H})$. We choose d = 100 and construct $\mathbf{H} = \mathbf{U}\boldsymbol{\Lambda}\mathbf{U}^{\top}$ with $\boldsymbol{\Lambda}$ log-uniform grid on $[10^{-2}, 10^2]$ and \mathbf{U} Haar-distributed. We set $\mathbf{w}^* = 0$, $F_* = 0$, and initialize $\mathbf{w}_1 \sim \mathcal{N}(0, 10^{-4}\mathbf{I})$, and report averages over 30 runs. To illustrate how individual eigenvalues affect constants $(\hat{L}, \hat{\mu}_{\mathrm{PL}}, K)$, we design three groups of tests targeting different part of the spectrum of \mathbf{H} .

Figure 2 shows how deflating different parts of the spectrum of \mathbf{H} affects the key theoretical constants. Denote the eigenpairs of \mathbf{H} as $(\lambda_i, \mathbf{u}_i)$, and let \mathbf{U}_s contain the selected eigenvectors. We construct a spectral preconditioner of the form $\mathbf{M} = \mathbf{I} + \mathbf{U}_s(\widetilde{\mathbf{\Lambda}}_s - \mathbf{I})\mathbf{U}_s^{\top}$, where $\widetilde{\mathbf{\Lambda}}_s = \operatorname{diag}(\tau_1, \dots, \tau_s)$ assigns a target value τ_i to the *i*-th chosen eigendirection. Deflating the largest s eigenvalues (left panel)—i.e., setting $\tau_i = \lambda_i$ so that these preconditioned eigenvalues become 1—reduces the smoothness constant \widehat{L} and the noise level $K = \frac{\sigma^2}{B} \operatorname{tr}(\mathbf{M}^{-1}\mathbf{H})$





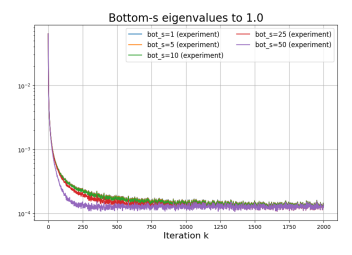


FIGURE 2. Convergence behavior under different deflation-based preconditioners. Left: deflating the largest s eigenvalues ($s \in \{1, 5, 10, 25, 50\}$). Middle: deflating the top 20 eigenvalues to target values 1.0, 2.0, 3.0, 5.0, 10.0]. Right: deflating the smallest s eigenvalues ($s \in \{1, 5, 10, 25, 50\}$).

while leaving $\hat{\mu}_{\text{PL}}$ unchanged, yielding a lower noise floor. To isolate the effect of the noise term, the middle panel fixes $\hat{\mu}_{\text{PL}}$. It deflates the top 20 eigenvalues into a common value v lying between λ_{21} and λ_d by setting $\tau_i = \lambda_i/v$, so that \hat{L} and $\hat{\mu}_{\text{PL}}$ remain unchanged while K varies. The resulting steady-state losses track this change in K, in line with the predicted noise-floor scaling. Deflating the smallest s eigenvalues (right panel)—that is, selecting the bottom eigenvectors and assigning target values τ_i equal to these smallest eigenvalues so that the preconditioned eigenvalues λ_i/τ_i move to 1—does increase $\hat{\mu}_{\text{PL}}$, but it simultaneously enlarges K. The two effects counterbalance each other, yielding only modest overall gains, consistent with the predicted noise-floor behavior.

SciML problems We then briefly summarize the three SciML tasks used to evaluate late–stage optimization behavior under different preconditioners.

Noisy Franke surface regression. The Franke function is a classical multiscale benchmark consisting of several Gaussian peaks with heterogeneous length scales. We sample 256 points uniformly in $[0,1]^2$ and corrupt the values with Gaussian noise $\varepsilon \sim \mathcal{N}(0,10^{-4})$. The combination of multiscale structure and observational noise yields a loss landscape with varying curvature, making it well suited for evaluating how preconditioning affects convergence in practice. The target surface is

$$f(x,y) = 0.75e^{-\frac{(9x-2)^2 + (9y-2)^2}{4}} + 0.75e^{-\frac{(9x+1)^2}{49} - \frac{9y+1}{10}} + 0.5e^{-\frac{(9x-7)^2 + (9y-3)^2}{4}} - 0.2e^{-(9x-4)^2 - (9y-7)^2}.$$

Physics-informed neural networks (PINNs). We train a PINN to solve the 2D Poisson problem

$$-\Delta u = f(x, y) = 8\pi^2 \sin(2\pi x) \sin(2\pi y)$$
 in $(0, 1)^2$, $u = 0$ on $\partial [0, 1]^2$,

whose exact solution is $u(x,y) = \sin(2\pi x)\sin(2\pi y)$. The training set includes 1,000 interior residual points and 200 boundary points. The weighted loss (PDE residual weight 1.0, boundary weight 100.0) produces a challenging composite landscape known to stress first-order methods [Krishnapriyan et al., 2021]. The right panel of Fig. 4 visualizes the source term f(x,y).

Green's-function learning. We learn Green's functions for the 1D convection-diffusion operator

$$\mathcal{L}u := -\nu u'' + \beta u', \qquad u(0) = u(1) = 0,$$

under two regimes: (i) diffusion-dominated ($\nu = 1.0, \beta = 0$) and (ii) convection-dominated ($\nu = 0.1, \beta = 1.0$). The Green's function satisfies $\mathcal{L}G(x,y) = \delta(x-y)$, where we approximate the delta distribution by a narrow Gaussian with width $\sigma = 0.01$. Training uses: (a) 1,000 uniformly sampled (x, y) pairs for PDE residuals, (b) 500 near-diagonal samples (|x-y| small) to capture

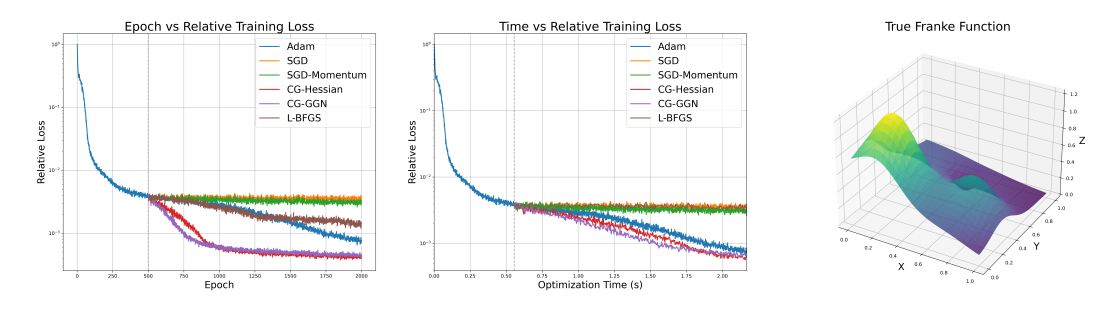


FIGURE 3. Franke-function regression (mean over 5 runs). Left: training loss vs. epochs with the switch to Phase II at epoch 500. Center: training loss vs. wall—clock time. Right: Franke surface.

the near-singularity, and (c) 200 boundary samples. This produces a highly multiscale and stiffness—dominated optimization problem, ideal for testing curvature-aware preconditioners. Baselines and protocol. Across all SciML tasks, we compare vanilla SGD, momentum, Adam, L—BFGS, and curvature-aware preconditioners (CG—Hessian and CG—GGN/Fisher). Matrix—free CG with a fixed iteration budget is used to apply Hessian or Gauss—Newton/Fisher updates. Following standard SciML practice, we adopt a two—phase schedule: Phase I uses Adam to reach a comparable basin; Phase II switches to the target optimizer to isolate late—stage behavior. We report loss vs. epochs and wall—clock time, with all architectural and implementation details in Appendix . All implementations use JAX [Bradbury et al., 2018]; code and data are available in the supplemental material.

Noisy data regression After the Adam warm start (Phase I), Phase II separates the methods (Fig. 3): Adam, L–BFGS, CG–GGN, and CG–Hessian descend faster than SGD and SGD+Momentum. The two curvature-aware variants, CG–Hessian and CG–GGN, track one another closely–showing similar contraction and reaching essentially the same loss floor. The similar performance of CG-Hessian and CG-GGN suggests that both methods provide comparable normal-space curvature and covariance matrix structure approximation. Adam's diagonal rescaling and L–BFGS's low-rank curvature information also mitigate anisotropy and stabilize noisy directions, which explains their advantage over SGD. In wall–clock time, the faster descent of curvature-aware methods compensates for their higher per-step cost.

Physics-informed neural networks (PINNs) With the same two-phase protocol, Phase II shows a consistent ranking (Fig. 4). At the bottom, Adam and SGD/SGD+Momentum lack explicit curvature information and progress slowly. L-BFGS achieves intermediate performance: it captures limited curvature through its low-rank approximation and line search, but the memory constraint prevents it from matching the full curvature captured by the two CG methods. At the top tier, CG-GGN and CG-Hessian both achieve better performance as curvature-aware methods, with CG-GGN showing a slight advantage.

For PINNs, which minimize weighted least-squares residuals, the Gauss-Newton approximation $\mathbf{J}^{\top}\mathbf{J}$ is naturally aligned with the gradient covariance structure and thus provides more effective noise attenuation—consistent with our theory, where the preconditioned noise level is governed by $\operatorname{tr}(\mathbf{M}^{-1}\boldsymbol{\Sigma}(\mathbf{w}))$ in the late stage. The Hessian approximation, by contrast, can introduce negative curvature and additional anisotropy. In wall-clock time, CG-GGN achieves the best accuracy within a comparable time budget, despite its higher per-step cost.

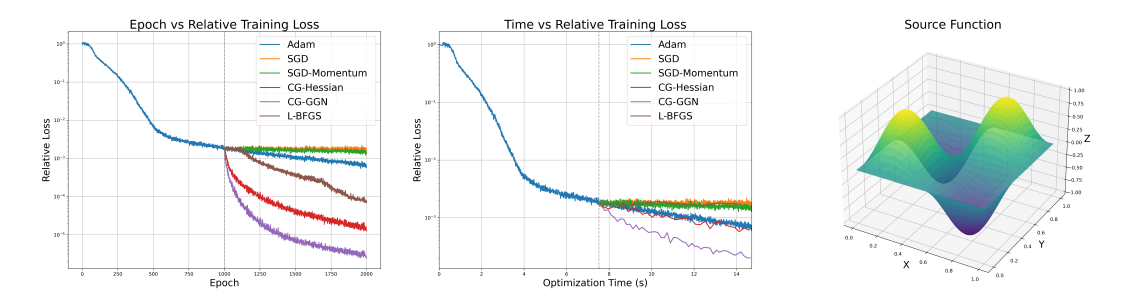


FIGURE 4. PINN for a Poisson-type PDE (mean over 5 runs). Left: training loss vs. epochs with Phase I \rightarrow Phase II at epoch 1,000. Center: training loss vs. wall—clock time. Right: source term.

Green's-function learning After Phase I, Phase II again shows a clear separation of methods (Figs. 5–6). In both the diffusion- and convection-dominated cases, CG-GGN continues to drive the loss down, whereas CG-Hessian, L-BFGS, Adam, SGD, and SGD+Momentum quickly form a tight cluster and improve only marginally. Compared with the earlier PINNs experiment, the Green's-function tasks are more near-singular due to the smoothed-delta forcing, leading to a more challenging, highly anisotropic optimization problem.

Although we did not directly measure the local constants $(\hat{L}, \hat{\mu}_{PL}, K)$ on this run, the observed advantage of CG–GGN is consistent with the structure of PINN objectives. First, for squared-residual losses, the Gauss–Newton/Fisher matrix is positive semidefinite, avoiding the negative-curvature directions introduced by second-derivative terms in the exact Hessian. This makes the preconditioner more stable and better suited to CG. Second, Fisher-type preconditioners are built from gradient second moments and therefore tend to whiten gradient noise, reducing the preconditioned noise level K. In contrast, a Hessian preconditioner includes second-order terms that are often misaligned with the gradient-noise covariance, and the damping needed to handle indefiniteness diminishes curvature gains while weakening noise attenuation.

These two effects—better alignment with useful curvature and more effective noise whitening—explain why CG–GGN reaches lower losses within comparable wall-clock time, despite its higher per-step cost.

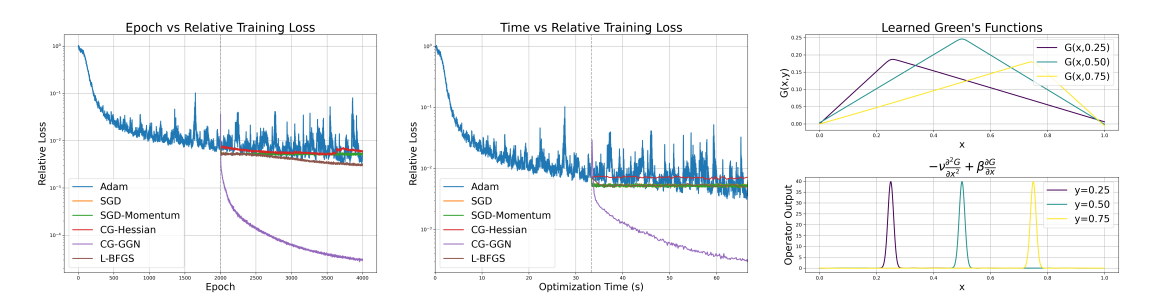


FIGURE 5. Laplacian Green's-function learning (mean over 5 runs). Left: loss vs. epochs with Phase I \rightarrow Phase II at epoch 2,000. Center: loss vs. wall-clock time. Right: learned G(x, y) for three source locations and operator checks.

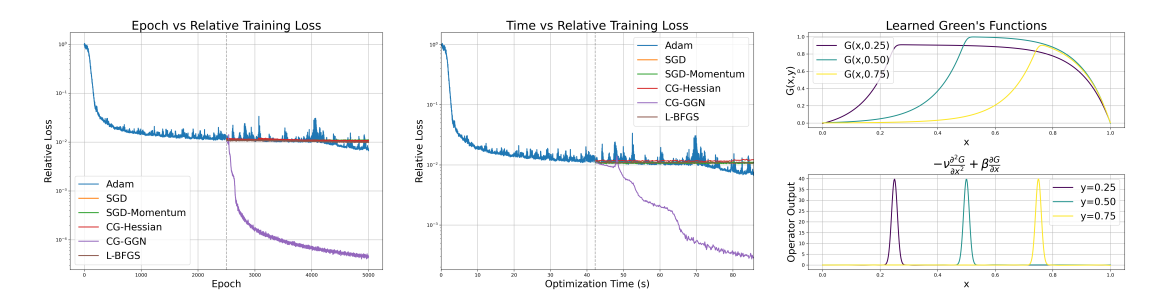


FIGURE 6. Convection–diffusion Green's-function learning (mean over 5 runs). Left: loss vs. epochs with Phase I \rightarrow Phase II at epoch 2,500. Center: loss vs. wall–clock time. Right: learned G(x,y) for three source locations and operator checks.

The right panels of Figs. 5 and 6 display the learned Green's functions G(x,y) at three representative source locations y together with simple operator and boundary checks for CG–GGN. The kernels are localized around the source locations and decay toward the Dirichlet boundaries, and the corresponding operator evaluations produce narrow spikes at x=y, in line with the smoothed–delta forcing used in the training loss. This suggests that the lower training losses achieved by CG–GGN reflect a reasonable Green's-function approximation rather than a purely numerical artifact.

Conclusion

We developed a local, geometry-aware theory for preconditioned SGD that makes two effects explicit: (1) the rate inside a basin is controlled by a preconditioner-dependent condition number in the \mathbf{M} -metric, and (2) the noise floor is governed by the preconditioned noise. We additionally obtained a basin-stability guarantee, giving an explicit probability that iterates remain in a region where these local properties hold. Together, the results motivate a simple rule: choose \mathbf{M} to improve local conditioning while suppressing noise in the \mathbf{M}^{-1} -norm.

A key next direction is *covariance-aware* preconditioning. Our bounds suggest that effective design should jointly target conditioning and noise attenuation, motivating structured covariance models and adaptive schemes that update curvature and noise statistics simultaneously. Extending basin-stability guarantees to nonstationary noise and developing online diagnostics for the local constants would move toward fully adaptive, geometry- and noise-aware SGD.

Acknowledgments

The research of M. Scott, T. Xu, and Y. Xi is supported by NSF DMS-2208412 and NSF DMS-2513118. The research of Q. Ye and A. Pichette-Emmons is supported by NSF DMS-2208314 and IIS-2327113. The research of Z. Tang and Y. Saad is supported by NSF DMS-2513117.

References

- Shunichi Amari. A theory of adaptive pattern classifiers. *IEEE Transactions on Electronic Computers*, EC-16(3):299-307, 1967. ISSN 0367-7508. doi: 10.1109/PGEC.1967.264666. URL https://ieeexplore.ieee.org/document/4039068. Conference Name: IEEE Transactions on Electronic Computers.
- Amit Attia and Tomer Koren. Sgd with adagrad stepsizes: Full adaptivity with high probability to unknown parameters, unbounded gradients and affine variance. In *International Conference on Machine Learning*, pages 1147–1171. PMLR, 2023.
- Francis Bach. Learning Theory from First Principles. The MIT Press, 2024. ISBN 9780262049443.
- David GT Barrett and Benoit Dherin. Implicit gradient regularization. arXiv preprint arXiv:2009.11162, 2020.
- Albert S. Berahas, Jorge Nocedal, and Martin Takáč. A multi-batch l-bfgs method for machine learning, 2016. URL https://arxiv.org/abs/1605.06049.
- Julius R. Blum. Approximation methods which converge with probability one. The Annals of Mathematical Statistics, 25(2):382-386, 1954. ISSN 0003-4851, 2168-8990. doi: 10.1214/aoms/1177728794. URL https://projecteuclid.org/journals/annals-of-mathematical-statistics/volume-25/issue-2/Approximation-Methods-which-Converge-with-Probability-one/10.1214/aoms/1177728794.full. Publisher: Institute of Mathematical Statistics.
- Raghu Bollapragada, Dheevatsa Mudigere, Jorge Nocedal, Hao-Jun Michael Shi, and Ping Tak Peter Tang. A progressive batching l-bfgs method for machine learning, 2018. URL https://arxiv.org/abs/1802.05374.
- Léon Bottou, Frank E. Curtis, and Jorge Nocedal. Optimization methods for large-scale machine learning. SIAM Review, 60(2):223-311, 2018. doi: 10.1137/16M1080173. URL https://doi.org/10.1137/16M1080173.
- James Bradbury, Roy Frostig, Peter Hawkins, Matthew James Johnson, Chris Leary, Dougal Maclaurin, George Necula, Adam Paszke, Jake VanderPlas, Skye Wanderman-Milne, and Qiao Zhang. JAX: composable transformations of Python+NumPy programs, 2018. URL http://github.com/jax-ml/jax.
- Han Chan. Some methods of unconstrained minimization. USSR Computational Mathematics and Mathematical Physics, 19(2):31-44, 1979. ISSN 0041-5553. doi: https://doi.org/10.1016/0041-5553(79)90004-1. URL https://www.sciencedirect.com/science/article/pii/0041555379900041.
- Jinghui Chen, Dongruo Zhou, Yiqi Tang, Ziyan Yang, Yuan Cao, and Quanquan Gu. Closing the generalization gap of adaptive gradient methods in training deep neural networks. In Christian Bessiere, editor, *Proceedings of the Twenty-Ninth International Joint Conference on Artificial Intelligence*, *IJCAI-20*, pages 3267–3275. International Joint Conferences on Artificial Intelligence Organization, 7 2020. doi: 10.24963/ijcai.2020/452. URL https://doi.org/10.24963/ijcai.2020/452. Main track.
- Weizhu Chen, Zhenghao Wang, and Jingren Zhou. Large-scale l-bfgs using mapreduce. In *Proceedings of the 28th International Conference on Neural Information Processing Systems* Volume 1, NIPS'14, page 1332–1340, Cambridge, MA, USA, 2014. MIT Press.
- John Duchi, Elad Hazan, and Yoram Singer. Adaptive subgradient methods for online learning and stochastic optimization. *Journal of Machine Learning Research*, 12:2121–2159, 2011.
- Matthew Faw, Isidoros Tziotis, Constantine Caramanis, Aryan Mokhtari, Sanjay Shakkottai, and Rachel Ward. The power of adaptivity in sgd: Self-tuning step sizes with unbounded

- gradients and affine variance. In Conference on Learning Theory, pages 313–355. PMLR, 2022.
- R. Fletcher. Practical Methods of Optimization. Wiley, 2013. ISBN 978-1-118-72318-0. URL https://books.google.com/books?id=_WuAvIx0EE4C.
- Francis Bach. Learning Theory from First Principles. Adaptive computation and machine learning series. MIT Press, 2 edition, 2024. ISBN 978-0-262-04944-3.
- Richard Franke. A Critical Comparison of Some Methods for Interpolation of Scattered Data. Technical report, Graduate School of Operational and Information Sciences (GSOIS), 1979. URL https://apps.dtic.mil/sti/citations/ADA081688.
- Sachin Garg, Albert S. Berahas, and Michał Dereziński. Second-order information promotes mini-batch robustness in variance-reduced gradients, 2024. URL https://arxiv.org/abs/2404.14758.
- Guillaume Garrigos and Robert M. Gower. Handbook of convergence theorems for (stochastic) gradient methods, 2024. URL http://arxiv.org/abs/2301.11235.
- Behrooz Ghorbani, Shankar Krishnan, and Ying Xiao. An investigation into neural net optimization via hessian eigenvalue density. In Kamalika Chaudhuri and Ruslan Salakhutdinov, editors, *Proceedings of the 36th International Conference on Machine Learning*, volume 97 of *Proceedings of Machine Learning Research*, pages 2232–2241. PMLR, 09–15 Jun 2019. URL https://proceedings.mlr.press/v97/ghorbani19b.html.
- Joshua D Griffin, Majid Jahani, Martin Takáč, Seyedalireza Yektamaram, and Wenwen Zhou. A minibatch stochastic Quasi-Newton method adapted for nonconvex deep learning problems. *Optimization Online*, 2022.
- Vineet Gupta, Tomer Koren, and Yoram Singer. Shampoo: Preconditioned stochastic tensor optimization. In Jennifer Dy and Andreas Krause, editors, *Proceedings of the 35th International Conference on Machine Learning*, volume 80 of *Proceedings of Machine Learning Research*, pages 1842–1850. PMLR, 10–15 Jul 2018. URL https://proceedings.mlr.press/v80/gupta18a.html.
- Wenrui Hao, Rui Peng Li, Yuanzhe Xi, Tianshi Xu, and Yahong Yang. Multiscale neural networks for approximating green's functions, 2024. URL https://arxiv.org/abs/2410.18439.
- Geoffrey Hinton. Neural networks for machine learning lecture 6e: rmsprop: Divide the gradient by a running average of its recent magnitude, 2014. URL https://www.cs.toronto.edu/~tijmen/csc321/slides/lecture_slides_lec6.pdf.
- Jared Kaplan, Sam McCandlish, Tom Henighan, Tom B. Brown, Benjamin Chess, Rewon Child, Scott Gray, Alec Radford, Jeffrey Wu, and Dario Amodei. Scaling laws for neural language models, 2020. URL https://arxiv.org/abs/2001.08361.
- Hamed Karimi, Julie Nutini, and Mark Schmidt. Linear convergence of gradient and proximal-gradient methods under the polyak-łojasiewicz condition. In Paolo Frasconi, Niels Landwehr, Giuseppe Manco, and Jilles Vreeken, editors, *Machine Learning and Knowledge Discovery in Databases*, pages 795–811, Cham, 2016. Springer International Publishing. ISBN 978-3-319-46128-1.
- Ahmed Khaled and Peter Richtárik. Better theory for SGD in the nonconvex world. Transactions on Machine Learning Research, 2023. ISSN 2835-8856. URL https://openreview.net/forum?id=AU4qHN2VkS. Survey Certification.
- Diederik P. Kingma and Jimmy Ba. Adam: A method for stochastic optimization, 2017. URL http://arxiv.org/abs/1412.6980.

- Tomer Koren, Roi Livni, Yishay Mansour, and Uri Sherman. Benign underfitting of stochastic gradient descent. Advances in Neural Information Processing Systems, 35:19605–19617, 2022.
- Aditi Krishnapriyan, Amir Gholami, Shandian Zhe, Robert Kirby, and Michael W Mahoney. Characterizing possible failure modes in physics-informed neural networks. In M. Ranzato, A. Beygelzimer, Y. Dauphin, P.S. Liang, and J. Wortman Vaughan, editors, Advances in Neural Information Processing Systems, volume 34, pages 26548–26560. Curran Associates, Inc., 2021. URL https://proceedings.neurips.cc/paper_files/paper/2021/file/df438e5206f31600e6ae4af72f2725f1-Paper.pdf.
- Frederik Kunstner, Lukas Balles, and Philipp Hennig. Limitations of the empirical fisher approximation for natural gradient descent. In *Proceedings of the 33rd International Conference on Neural Information Processing Systems*, Red Hook, NY, USA, 2019. Curran Associates Inc.
- Susanna Lange, Kyle Helfrich, and Qiang Ye. Batch normalization preconditioning for neural network training. *Journal of Machine Learning Research*, 23(72):1–41, 2022.
- Xi-Lin Li. Preconditioned stochastic gradient descent. *IEEE Transactions on Neural Networks and Learning Systems*, 29(5):1454–1466, 2018. doi: 10.1109/TNNLS.2017.2672978.
- Dong C. Liu and Jorge Nocedal. On the limited memory BFGS method for large scale optimization. *Mathematical Programming*, 45(1):503–528, August 1989. ISSN 1436-4646. doi: 10.1007/BF01589116. URL https://doi.org/10.1007/BF01589116.
- Hong Liu, Zhiyuan Li, David Leo Wright Hall, Percy Liang, and Tengyu Ma. Sophia: A scalable stochastic second-order optimizer for language model pre-training. In *The Twelfth International Conference on Learning Representations*, 2024. URL https://openreview.net/forum?id=3xHDeA8Noi.
- Ilya Loshchilov and Frank Hutter. Decoupled weight decay regularization. arXiv preprint arXiv:1711.05101, 2017.
- James Martens. New insights and perspectives on the natural gradient method. *Journal of Machine Learning Research*, 21(146):1-76, 2020. URL http://jmlr.org/papers/v21/17-678.html.
- James Martens and Roger Grosse. Optimizing neural networks with kronecker-factored approximate curvature. In *Proceedings of the 32nd International Conference on International Conference on Machine Learning Volume 37*, ICML'15, page 2408–2417. JMLR.org, 2015.
- Pratik Rathore, Weimu Lei, Zachary Frangella, Lu Lu, and Madeleine Udell. Challenges in training pinns: a loss landscape perspective. In *Proceedings of the 41st International Conference on Machine Learning*, ICML'24. JMLR.org, 2024.
- Sashank J. Reddi, Satyen Kale, and Sanjiv Kumar. On the convergence of adam and beyond. In *International Conference on Learning Representations*, 2018. URL https://openreview.net/forum?id=ryQu7f-RZ.
- Herbert Robbins and Sutton Monro. A stochastic approximation method. AnnalsofMathematicalStatistics, 22(3):400-407, 1951.ISSN 10.1214/aoms/1177729586. 2168-8990. doi: URL https://projecteuclid. org/journals/annals-of-mathematical-statistics/volume-22/issue-3/ A-Stochastic-Approximation-Method/10.1214/aoms/1177729586.full. Publisher:
 - Institute of Mathematical Statistics.

 event Sagun Utku Evci V Ugur Guney Vann Dauphin, and Leon Bottou. Empirical analysis
- Levent Sagun, Utku Evci, V. Ugur Guney, Yann Dauphin, and Leon Bottou. Empirical analysis of the hessian of over-parametrized neural networks, 2018. URL https://openreview.net/forum?id=rJrTwxbCb.

- Robin M Schmidt, Frank Schneider, and Philipp Hennig. Descending through a crowded valley benchmarking deep learning optimizers. In Marina Meila and Tong Zhang, editors, Proceedings of the 38th International Conference on Machine Learning, volume 139 of Proceedings of Machine Learning Research, pages 9367–9376. PMLR, 18–24 Jul 2021. URL https://proceedings.mlr.press/v139/schmidt21a.html.
- Frank Schneider, Lukas Balles, and Philipp Hennig. DeepOBS: A deep learning optimizer benchmark suite. In *International Conference on Learning Representations*, 2019. URL https://openreview.net/forum?id=rJg6ssC5Y7.
- Nicol N. Schraudolph. Fast curvature matrix-vector products for second-order gradient descent. Neural Computation, 14(7):1723-1738, 2002. ISSN 0899-7667, 1530-888X. doi: 10.1162/08997660260028683. URL https://direct.mit.edu/neco/article/14/7/ 1723-1738/6626.
- Kevin Swersky, Marc'Aurelio Ranzato, David Buchman, Benjamin Marlin, and Nando Freitas. On autoencoders and score matching for energy based models. In Lise Getoor and Tobias Scheffer, editors, *Proceedings of the 28th International Conference on Machine Learning (ICML-11)*, ICML '11, pages 1201–1208, New York, NY, USA, June 2011. ACM. ISBN 978-1-4503-0619-5. URL http://mldiscuss.appspot.com/venue/ICML/2011/article/622/.
- Tianshi Xu, Rui Peng Li, and Yuanzhe Xi. Neural approximate inverse preconditioners, 2025. URL https://arxiv.org/abs/2510.13034.
- Qiang Ye. Preconditioning for accelerated gradient descent optimization and regularization, 2024. URL https://arxiv.org/abs/2410.00232.
- Manzil Zaheer, Sashank Reddi, Devendra Sachan, Satyen Kale, and Sanjiv Kumar. Adaptive methods for nonconvex optimization. In S. Bengio, H. Wallach, H. Larochelle, K. Grauman, N. Cesa-Bianchi, and R. Garnett, editors, *Advances in Neural Information Processing Systems*, volume 31. Curran Associates, Inc., 2018. URL https://proceedings.neurips.cc/paper_files/paper/2018/file/90365351ccc7437a1309dc64e4db32a3-Paper.pdf.
- Handi Zhang, Langchen Liu, and Lu Lu. Federated scientific machine learning for approximating functions and solving differential equations with data heterogeneity, 2024. URL https://arxiv.org/abs/2410.13141.

Appendix

Notation used in paper

In general, capital bold letters are matrices (**A**), lower case bold letters are vectors (**v**), and lower case Greek or Latin letters are constants (ν , c). Moreover, there are some notation that is used consistently throughout the paper. A reference table for these symbols is given in Table 1.

Table 1. Reference for recurring notation in the paper.

Symbol	Definition
k	iteration counter
w	Model parameters
$F(\mathbf{w})$	Objective function at point w
$F_* := F(\mathbf{w}^*)$	minimum function value at minimizer
α	learning rate
α_k	learning rate scheduler/ learning rate at epoch k
$\overline{\alpha}$	fixed learning rate
c, L	strong convexity, Lipschitz constant for $\left\ \cdot\right\ _2 = \left\ \cdot\right\ _{\mathbf{I}}$
\hat{c},\hat{L}	strong convexity, Lipschitz constant for preconditioned case: $\ \cdot\ _{\mathbf{M}}$
$\hat{\mu}_{PL}$	PL constant for preconditioned case: $\ \cdot\ _{\mathbf{M}}$
\mathcal{B}	mini-batch of the dataset
M	generic preconditioner where \mathbf{M}^{-1} is applied to a vector
$g(\cdot,\cdot)$	gradient vector
$\kappa(\mathbf{M})$	Condition number of M (always based on $\ \cdot\ _2$)
μ, μ_G	lower and upper bound constants on the first moment of the gradient
K, K_V	constant and scaling values of the affine bound on the gradient's variance
K_G	Constant needed for learning rate upper bound, dependent on $K_V + \mu_G^2 > 0$.
$\mathbb{E}_{oldsymbol{\xi}}, \mathbb{V}_{oldsymbol{\xi}}$	Expectation and Variance of gradient with random realization $\boldsymbol{\xi}$
β, γ	constants affecting the lower and upper bound on α_k for diminishing learning rate proofs
ν	convergence constant in $\mathcal{O}((\gamma+k)^{-1})$
r	radius of convex basin around local minimum
$\mathcal{N}_r, \mathcal{N}_{r_+}$	local neighborhood around minimizer, slightly larger local neighborhood for containment
τ	smallest iteration number where $\mathbf{w}_k \notin \mathcal{N}_r$.
C	The stochastic noise floor defined $\bar{\alpha}\hat{L}K/(2\hat{c}\mu)$
$\mathcal{N}_{\mathbf{M}}(\mathbf{w})$	instantaneous preconditioned noise $\operatorname{tr}(\mathbf{M}^{-1}\Sigma(\mathbf{w}))$
K	uniform baseline for $\mathcal{N}_{\mathbf{M}}(\mathbf{w})$ on the analysis region (noise floor constant)
$lpha_{ m QG}$	quadratic growth constant of locally convex basin a distance from the minimizer

Mathematical preliminaries

Preconditioning The condition number from a linear equation $\mathbf{A}\mathbf{x} = \mathbf{b}$ bounds the accuracy of the solution \mathbf{x} , and is defined as

$$\kappa(\mathbf{A}) = \|\mathbf{A}\| \|\mathbf{A}^{-1}\|,$$

where if not stated $\|\cdot\| = \|\cdot\|_2$. If **A** is ill-conditioned, i.e. has a large condition number, then a small perturbation in **b** can result in a large perturbation of the solution **x**. In addition to the accuracy of the solution, the convergence rate of iterative methods, such as conjugate gradient, depends on $r = \frac{\sqrt{\kappa} - 1}{\sqrt{\kappa} + 1}$.

It is easy to see that r < 1, but if $\kappa \gg 1$, then convergence will be extremely slow as $r \to 1$. This motivates the need for ways to reduce the condition number, through a technique called *preconditioning*. Throughout this paper, we assume that **M** is the preconditioner, and we only

have access to the action of M^{-1} onto a vector. More technically, we say M is an efficient preconditioner to the matrix A such that

$$\kappa(\mathbf{M}^{-1}\mathbf{A}) < \kappa(\mathbf{A}).$$

For clarity, even though we call \mathbf{M} the preconditioner, we don't explicitly form it. Additionally, we don't form \mathbf{M}^{-1} either but just observe the action of the preconditioner on a vector, $\mathbf{M}^{-1}\mathbf{v}$.

There are different ways we can utilize the preconditioner \mathbf{M} . First, assume \mathbf{M}^{-1} exists, then the *left* preconditioned system is

$$\mathbf{M}^{-1}\left(\mathbf{A}\mathbf{x} - \mathbf{b}\right) = 0.$$

Both the original linear system and the left-preconditioned system give the same solution. Additionally, we could solve the right preconditioned system

$$\mathbf{A}\mathbf{M}^{-1}\left(\mathbf{M}\mathbf{x}\right) = \mathbf{b}.$$

This requires us to solve $\mathbf{A}\mathbf{M}^{-1}\mathbf{y} = \mathbf{b}$ for \mathbf{y} , and then to recover the original solution, we would need to do another linear system solve $\mathbf{M}\mathbf{x} = \mathbf{y}$ for \mathbf{x} .

These two techniques can be combined to perform split preconditioning. If we employ M as the right preconditioner, and N as the left preconditioner, we compute

$$\mathbf{NAM}^{-1}\left(\mathbf{Mx}\right) = \mathbf{Nb}.$$

This is beneficial if one would like to scale the rows and columns of \mathbf{A} differently. Additionally, observe that if \mathbf{A} is symmetric and $\mathbf{N}^{\top} = \mathbf{M}^{-1}$, then $\mathbf{N}\mathbf{A}\mathbf{M}^{-1}$ is also symmetric.

In the preconditioned version of CG (PCG), one solves the equivalent system $\mathbf{M}^{-1}\mathbf{A}\mathbf{x} = \mathbf{M}^{-1}\mathbf{b}$ using a similar three-term recurrence, but applied to the transformed system. The key requirement is that the preconditioner \mathbf{M} be symmetric positive definite and chosen so that $\mathbf{M}^{-1}\mathbf{A}$ has a significantly smaller condition number than \mathbf{A} itself. For practical purposes, PCG is used in matrix-free settings where only the action $\mathbf{M}^{-1}\mathbf{v}$ is required, not the explicit matrix \mathbf{M}^{-1} .

Preconditioners for SGD In this section, we briefly review several preconditioners commonly used in the ML literature. First, if we define \mathbf{s}_k to be the sum of the squared gradients up until iteration k, we arrive at AdaGrad [Duchi et al., 2011]

$$\mathbf{M}_{\text{AdaGrad}} = \operatorname{diag}\left(\sqrt{\mathbf{s}_k} + \varepsilon\right).$$

The issues with this is the gradient squared will only increase, leading to premature stopping. To counteract that, exponentially moving weighted averages are widely used in diagonal preconditioners such as Adam [Kingma and Ba, 2017] and its momentum-less counterpart RMSProp [Hinton, 2014]:

$$\mathbf{M}_{\mathrm{Adam}} = \mathrm{diag}\left(\sqrt{\mathbf{s}_k} + \varepsilon\right),$$

where here \mathbf{s}_k is an exponential moving average of squared gradients, and $\varepsilon > 0$ is a small constant added for numerical stability. While computationally efficient and robust to scaling, such diagonal preconditioners fail to capture cross-parameter curvature, which may lead to suboptimal convergence in ill-conditioned problems.

The Hessian matrix of the loss function,

$$\mathbf{H}(\mathbf{w}) = \nabla^2 \mathcal{L}(\mathbf{w}),$$

captures the exact second-order structure of the problem and provides the most complete curvature information. However, computing or storing the full Hessian is typically infeasible in high-dimensional neural network (NN) models. Moreover, it is not guaranteed to be positive definite in nonconvex settings, which complicates its direct use as a preconditioner.

To reduce computational cost, one can approximate the Hessian using a single mini-batch, \mathcal{B} :

$$\mathbf{H}_{\mathcal{B}}(\mathbf{w}) = \nabla^2 \mathcal{L}_{\mathcal{B}}(\mathbf{w}).$$

This matrix is cheaper to compute and can be updated online, but suffers from high variance and may not preserve important curvature directions observed over the full dataset. While the Newton and quasi-Newton methods work well for deterministic optimization, many have provided a distinction between these and other methods for designing preconditioners in the stochastic setting [Li, 2018, Bottou et al., 2018].

As opposed to constructing the Hessian, an alternative is the Gauss-Newton Hessian approximation, which assumes the difference between the model and label is small in a least-squares norm. This idea was further generalized to loss functions of the form $\ell(\theta) = \sum_n a_n (b_n(\theta))$ in Schraudolph [2002]. This generalized Gauss-Newton matrix (GGN), which ignores second order information of b_n , is SPD when a_n is convex even when the true Hessian is indefinite.

Another alternate method is the FIM defined as

$$\mathbf{F}(\mathbf{w}) = \mathbb{E}_{x,y} \left[\nabla_{\mathbf{w}} \log p_{\mathbf{w}}(y \mid x) \nabla_{\mathbf{w}} \log p_{\mathbf{w}}(y \mid x)^{\top} \right],$$

which is guaranteed to be SPD under mild regularity conditions. For models trained with exponential-family losses, the FIM coincides with the GGN [Martens, 2020, Schraudolph, 2002]. Its structure allows for stable and curvature-aware preconditioning.

The empirical FIM estimates the expectation in the FIM using a finite mini-batch:

$$\mathbf{F}_{\mathrm{emp}}(\mathbf{w}) = \frac{1}{|\mathcal{B}|} \sum_{(x,y) \in \mathcal{B}} \nabla_{\mathbf{w}} \log p_{\mathbf{w}}(y \mid x) \nabla_{\mathbf{w}} \log p_{\mathbf{w}}(y \mid x)^{\top}.$$

It is symmetric and positive semidefinite, and is often used in practice due to its lower computational overhead compared to the full FIM. However, it may introduce bias depending on the mini-batch size and model quality [Kunstner et al., 2019].

Finally, the L-BFGS algorithm is a popular quasi-Newton method that builds a low-rank approximation to the inverse Hessian using a history of gradients and iterates. It is well-suited to medium-scale problems and has seen empirical success in ML [Bottou et al., 2018]. Additional variants of L-BFGS have also been proposed [Berahas et al., 2016, Bollapragada et al., 2018]. While not traditionally framed as a preconditioner, L-BFGS can be interpreted as implicitly applying a data-driven curvature approximation.

Assumptions and proofs of theorems

Assumptions

Assumption 9 (Strong Convexity). The objective function $F: \mathbb{R}^d \to \mathbb{R}$ is strongly convex in that there exists a constant c > 0 such that

$$F(\overline{\mathbf{w}}) \ge F(\mathbf{w}) + \nabla F(\mathbf{w})^{\top} (\overline{\mathbf{w}} - \mathbf{w}) + \frac{1}{2} c ||\overline{\mathbf{w}} - \mathbf{w}||_{2}^{2}, \qquad \forall \ (\overline{\mathbf{w}}, \mathbf{w}) \in \mathbb{R}^{d} \times \mathbb{R}^{d}$$

From elementary optimization, this assumption is equivalent to F having a unique minimizer $\mathbf{w}^* \in \mathbb{R}^d$. We define $F_* := F(\mathbf{w}^*)$.

Assumption 10 (Lipschitz continuity of gradient). The objective function $F: \mathbb{R}^d \to \mathbb{R}$ is continuously differentiable and the gradient function of $F, \nabla F: \mathbb{R}^d \to \mathbb{R}^d$, is Lipschitz continuous with Lipschitz constant L > 0, i.e.

$$||\nabla F(\mathbf{w}) - \nabla F(\overline{\mathbf{w}})||_2 \le L||\mathbf{w} - \overline{\mathbf{w}}||_2$$

for all $\{\mathbf{w}, \overline{\mathbf{w}}\} \subset \mathbb{R}^d$.

Remark 1. If F is continuously twice differentiable, then ∇F is Lipschitz continuous with Lipschitz constant L if and only if the eigenvalues of the matrix $\nabla^2 F(\mathbf{w})$ are bounded above by L for all w. F is strongly convex with constant c if and only if the eigenvalues of the matrix $\nabla^2 F(\mathbf{w})$ is bounded below by c for all w. Therefore, L/c is an upper bound of the condition number of $\nabla^2 F(\mathbf{w})$.

Lipschitz continuity of gradient is an assumption made in nearly all convergence analyses of gradient-based methods [Khaled and Richtárik, 2023].

Assumption 11 (Bounds on First and Second Moments of Gradient). Assume

(1) There exist scalars $\mu_G \ge \mu > 0$ such that, for all $k \in \mathbb{N}$,

(9)
$$\nabla F(\mathbf{w}_k)^{\top} \mathbb{E}_{\boldsymbol{\xi}_k}[g(\mathbf{w}_k, \boldsymbol{\xi}_k)] \ge \mu ||\nabla F(\mathbf{w}_k)||_2^2$$

(10)
$$||\mathbb{E}_{\boldsymbol{\xi}_k}[g(\mathbf{w}_k, \boldsymbol{\xi}_k)]||_2 \le \mu_G ||\nabla F(\mathbf{w}_k)||_2$$

(2) There exist scalars $K \geq 0$ and $K_V \geq 0$ such that, for all $k \in \mathbb{N}$,

(11)
$$\mathbb{V}_{\boldsymbol{\xi}_k}[g(\mathbf{w}_k, \boldsymbol{\xi}_k)] \le K + K_V ||\nabla F(\mathbf{w}_k)||_2^2$$

where
$$\mathbb{V}_{\xi_k}[g(\mathbf{w}_k, \xi_k)] := \mathbb{E}_{\xi_k}[||g(\mathbf{w}_k, \xi_k)||_2^2] - ||\mathbb{E}_{\xi_k}[g(\mathbf{w}_k, \xi_k)]||_2^2$$
.

Theorem 6 (Strongly convex objective function, fixed learning rate [Bottou et al., 2018]). Under Assumptions 9,10, 11, suppose that the SGD algorithm is run with fixed learning rates, $\alpha_k = \overline{\alpha}$ for all $k \in \mathbb{N}$ where

$$0 < \overline{\alpha} \le \frac{\mu}{LK_G}$$
 and $K_G := K_V + \mu_G^2 \ge \mu^2 > 0$.

Then, the expected optimality gap satisfies the following for all $k \in \mathbb{N}$:

(12)
$$\mathbb{E}[F(\mathbf{w}_k) - F_*] \le \frac{\overline{\alpha}LK}{2c\mu} + (1 - \overline{\alpha}c\mu)^{k-1} \left(F(\mathbf{w}_1) - F_* - \frac{\overline{\alpha}LK}{2c\mu} \right) \stackrel{k \to \infty}{\longrightarrow} \frac{\overline{\alpha}LK}{2c\mu}$$

Note that it follows from (10) and (11) that $\mathbb{E}_{\boldsymbol{\xi}_k}[||g(\mathbf{w}_k, \boldsymbol{\xi}_k)||_2^2] \leq K + K_G ||\nabla F(\mathbf{w}_k)||_2^2$ with $K_G := K_V + \mu_G^2 \geq \mu^2 > 0$.

Theorem 7 (Strongly convex objective function, diminishing learning rates [Bottou et al., 2018]). Under the same assumptions as Theorem 6, suppose that the SGD algorithm is run with a learning rate sequence such that, for all $k \in \mathbb{N}$,

$$\alpha_k = \frac{\beta}{\gamma + k}$$
 for some $\beta > \frac{1}{c\mu}$ and $\gamma > 0$ such that $\alpha_1 \leq \frac{\mu}{LK_G}$

Then, the expected optimality gap satisfies the following for all $k \in \mathbb{N}$:

(13)
$$\mathbb{E}[F(\mathbf{w}_k) - F_*] \le \frac{\nu}{\gamma + k}$$

where

(14)
$$\nu := \max \left\{ \frac{\beta^2 LK}{2(\beta c\mu - 1)}, (\gamma + 1)(F(\mathbf{w}_1) - F_*) \right\}$$

Under the assumption of strong convexity, the optimality gap can be bounded at any point by the 2-norm squared of the gradient of the objective function at that particular point. That is

$$2c(F(\mathbf{w}) - F_*) \leq ||\nabla F(\mathbf{w})||_2^2 \text{ for all } \mathbf{w} \in \mathbb{R}^d$$

As before, F has a unique minimizer, denoted as $\mathbf{w}^* \in \mathbb{R}^d$ with $F_* := F(\mathbf{w}^*)$.

Previously, the optimality gap was bounded by the 2-norm of the gradient of the objective function squared. Here, however, the optimality gap is bounded by the \mathbf{M} -norm of the gradient of the objective function squared. That is,

$$2\hat{c}(F(\mathbf{w}) - F(\mathbf{w}_*)) \le ||\nabla F(\mathbf{w})||_{\mathbf{M}^{-1}}^2$$

This result is used several times in the upcoming proofs. We repeat Lemma 1 here for convenience below:

Lemma 8. Let F be twice differentiable and $\mathbf{M}^{-1} = \mathbf{P}\mathbf{P}^{\top}$. Then: (i) ∇F is \mathbf{M} -Lipschitz with constant $\hat{L} \iff$ all eigenvalues of $\mathbf{P}^{\top}\nabla^{2}F(\mathbf{w})\mathbf{P}$ are $\leq \hat{L}$; (ii) F is \mathbf{M} -strongly convex with constant $\hat{c} \iff$ all eigenvalues of $\mathbf{P}^{\top}\nabla^{2}F(\mathbf{w})\mathbf{P}$ are $\geq \hat{c}$.

Proof. We consider a change of parameter as used in preconditioning. Let $\mathbf{w} = \mathbf{Pz}$ and $\overline{\mathbf{w}} = \mathbf{P}\overline{\mathbf{z}}$. Then $\mathbf{w} - \overline{\mathbf{w}} = \mathbf{P}(\mathbf{z} - \overline{\mathbf{z}})$ which gives $\mathbf{P}^{-1}(\mathbf{w} - \overline{\mathbf{w}}) = \mathbf{z} - \overline{\mathbf{z}}$. Define $f(\mathbf{z}) = F(\mathbf{Pz})$. Then $\nabla_{\mathbf{z}} f(\mathbf{z}) = \mathbf{P}^{\top} \nabla_{\mathbf{w}} F(\mathbf{w})$ and $\nabla_{\mathbf{z}}^{2} f(z) = \mathbf{P}^{\top} \nabla_{\mathbf{w}}^{2} F(\mathbf{w}) \mathbf{P}$. Hence

$$||\nabla f(\mathbf{z}) - \nabla f(\overline{\mathbf{z}})||_2 = ||\mathbf{P}^{\top} \nabla_{\mathbf{w}} F(\mathbf{w}) - \mathbf{P}^{\top} \nabla_{\mathbf{w}} F(\overline{\mathbf{w}})||_2 = ||\nabla_{\mathbf{w}} F(\mathbf{w}) - \nabla_{\mathbf{w}} F(\overline{\mathbf{w}})||_{\mathbf{M}^{-1}}.$$

Therefore, the M-Lipschitz continuity of the gradient for F is equivalent to the Lipschitz continuity of the gradient for f, which is equivalent to that $\nabla_z^2 f(z)$, i.e. $\mathbf{P}^{\top} \nabla_w^2 F(\mathbf{w}) \mathbf{P}$, has eigenvalues bounded above by \hat{L} . Similarly, the statement on M-strong convexity follows from

$$F(\mathbf{w}) + \nabla F(\mathbf{w})^{\top} (\overline{\mathbf{w}} - \mathbf{w}) + \frac{1}{2} \hat{c} ||\overline{\mathbf{w}} - \mathbf{w}||_{\mathbf{M}}^{2} = f(\mathbf{z}) + \nabla_{\mathbf{z}} f(\mathbf{z})^{\top} (\overline{\mathbf{z}} - \mathbf{z}) + \frac{1}{2} \hat{c} ||\overline{\mathbf{z}} - \mathbf{z}||_{2}^{2}.$$

We may assume \hat{L} and \hat{c} are respectively the maximum and the minimum of the eigenvalues of $\mathbf{P}^{\top}\nabla^{2}F(\mathbf{w})\mathbf{P}$ for all \mathbf{w} . So $\frac{\hat{L}}{\hat{c}}$ plays the role of the condition number of the preconditioned matrix $\mathbf{P}^{\top}\nabla^{2}F(\mathbf{w})\mathbf{P}$. If we assume $\mathbf{M}^{-1} = \mathbf{P}\mathbf{P}^{\top}$ is such that $\frac{\hat{L}}{\hat{c}}$ is smaller than $\frac{L}{c}$, it basically reduces the condition number. We will demonstrate that this accelerates the speed of convergence.

An important lemma comes directly from this assumption.

Lemma 9. Under the assumption of M-Lipschitz continuity of gradient,

(15)
$$F(\mathbf{w}) \le F(\overline{\mathbf{w}}) + \nabla F(\overline{\mathbf{w}})^{\top} (\mathbf{w} - \overline{\mathbf{w}}) + \frac{1}{2} \hat{L} ||\mathbf{w} - \overline{\mathbf{w}}||_{\mathbf{M}}^{2}$$

Proof. Consider the following,

$$F(\mathbf{w}) = F(\overline{\mathbf{w}}) + \int_0^1 (\nabla F(\overline{\mathbf{w}} + t(\mathbf{w} - \overline{\mathbf{w}}))^{\top} \mathbf{P} \mathbf{P}^{-1}(\mathbf{w} - \overline{\mathbf{w}}) dt$$

$$= F(\overline{\mathbf{w}}) + \nabla F(\overline{\mathbf{w}})^{\top} (\mathbf{w} - \overline{\mathbf{w}}) + \int_0^1 (\nabla F(\overline{\mathbf{w}} + t(\mathbf{w} - \overline{\mathbf{w}})) - \nabla F(\overline{\mathbf{w}}))^{\top} \mathbf{P} \mathbf{P}^{-1}(\mathbf{w} - \overline{\mathbf{w}}) dt$$

$$\leq F(\overline{\mathbf{w}}) + \nabla F(\overline{\mathbf{w}})^{\top} (\mathbf{w} - \overline{\mathbf{w}}) + \int_0^1 \hat{L} ||t(\mathbf{w} - \overline{\mathbf{w}})||_{\mathbf{M}} ||\mathbf{w} - \overline{\mathbf{w}}||_{\mathbf{M}} dt$$

which gives us our consequence that was to be shown.

Notice that combining the variance definition (Eq. 3) with Assumption 3, we have the following

(16)
$$\mathbb{E}_{\boldsymbol{\xi}_k}[||g(\mathbf{w}_k, \boldsymbol{\xi}_k)||_{\mathbf{M}^{-1}}^2] \leq K_G ||\nabla F(\mathbf{w}_k)||_{\mathbf{M}^{-1}}^2 + K \text{ with } K_G := K_V + \mu_G^2 \geq \mu^2 > 0$$
 The proof for the two theorems relies on the following lemmas.

Lemma 10. Under Assumption 1, the iterates of Eq. 2 satisfy the following inequality for all $k \in \mathbb{N}$:

(17)
$$\mathbb{E}_{\boldsymbol{\xi}_k}[F(\mathbf{w}_{k+1})] - F(\mathbf{w}_k) \leq -\alpha_k \nabla F(\mathbf{w}_k)^{\top} \mathbb{E}_{\boldsymbol{\xi}_k}[g(\mathbf{w}_k, \boldsymbol{\xi}_k)] + \frac{1}{2} \alpha_k^2 \hat{L} \mathbb{E}_{\boldsymbol{\xi}_k}[||g(\mathbf{w}_k, \boldsymbol{\xi}_k)||_{\mathbf{M}^{-1}}^2]$$

Proof. Let $\mathbf{w} = \mathbf{w}_{k+1}$ and $\overline{\mathbf{w}} = \mathbf{w}_k$. Then, by Assumption 1,

$$F(\mathbf{w}_{k+1}) - F(\mathbf{w}_k) \le \nabla F(\mathbf{w}_k)^{\top} (\mathbf{w}_{k+1} - \mathbf{w}_k) + \frac{1}{2} \hat{L} ||\mathbf{w}_{k+1} - \mathbf{w}_k||_{\mathbf{M}}^2$$

Recalling that Eq. 2 gives $\mathbf{w}_{k+1} = \mathbf{w}_k - \alpha_k \mathbf{M}^{-1} g(\mathbf{w}_k, \boldsymbol{\xi}_k)$, we then have,

$$F(\mathbf{w}_{k+1}) - F(\mathbf{w}_k) \leq \nabla F(\mathbf{w}_k)^{\top} (-\alpha_k \mathbf{M}^{-1} g(\mathbf{w}_k, \boldsymbol{\xi}_k)) + \frac{1}{2} \hat{L} || -\alpha_k \mathbf{M}^{-1} g(\mathbf{w}_k, \boldsymbol{\xi}_k) ||_{\mathbf{M}}^{2}$$

$$\leq -\alpha_k \nabla F(\mathbf{w}_k)^{\top} \mathbf{M}^{-1} g(\mathbf{w}_k, \boldsymbol{\xi}_k) + \frac{1}{2} \alpha_k^2 \hat{L} || \mathbf{M}^{-1} g(\mathbf{w}_k, \boldsymbol{\xi}_k) ||_{\mathbf{M}}^{2}$$

$$\leq -\alpha_k \nabla F(\mathbf{w}_k)^{\top} \mathbf{M}^{-1} g(\mathbf{w}_k, \boldsymbol{\xi}_k) + \frac{1}{2} \alpha_k^2 \hat{L} || g(\mathbf{w}_k, \boldsymbol{\xi}_k) ||_{\mathbf{M}^{-1}}^{2}$$

Take the expectation of both sides

$$\mathbb{E}_{\boldsymbol{\xi}_k}[F(\mathbf{w}_{k+1})] - F(\mathbf{w}_k) \le -\alpha_k \nabla F(\mathbf{w}_k)^{\top} \mathbf{M}^{-1} \mathbb{E}_{\boldsymbol{\xi}_k}[g(\mathbf{w}_k, \boldsymbol{\xi}_k)] + \frac{1}{2} \alpha_k^2 \hat{L} \mathbb{E}_{\boldsymbol{\xi}_k}[||g(\mathbf{w}_k, \boldsymbol{\xi}_k)||_{\mathbf{M}^{-1}}^2]$$
Thus, the desired result is achieved.

Lemma 11. Under Assumptions 1 and 2, the iterates of Eq. 2 satisfy the following inequalities for all $k \in \mathbb{N}$:

(18)
$$\mathbb{E}_{\boldsymbol{\xi}_k}[F(\mathbf{w}_{k+1})] - F(\mathbf{w}_k) \le -\mu\alpha_k ||\nabla F(\mathbf{w}_k)||_{\mathbf{M}^{-1}}^2 + \frac{1}{2}\alpha_k^2 \hat{L} \mathbb{E}_{\boldsymbol{\xi}_k} \left[||g(\mathbf{w}_k, \boldsymbol{\xi}_k)||_{\mathbf{M}^{-1}}^2 \right]$$

$$\leq -(\mu - \frac{1}{2}\alpha_k \hat{L}K_G)\alpha_k ||\nabla F(\mathbf{w}_k)||_{\mathbf{M}^{-1}}^2 + \frac{1}{2}\alpha_k^2 \hat{L}K_G$$

Proof. By Lemma 10 and Assumption 2, it follows that

$$\mathbb{E}_{\boldsymbol{\xi}_{k}}[F(\mathbf{w}_{k+1})] - F(\mathbf{w}_{k}) \leq -\alpha_{k}\mu||\nabla F(\mathbf{w}_{k})||_{\mathbf{M}^{-1}}^{2} + \frac{1}{2}\alpha_{k}^{2}\hat{L}\mathbb{E}_{\boldsymbol{\xi}_{k}}\left[||g(\mathbf{w}_{k},\boldsymbol{\xi}_{k})||_{\mathbf{M}^{-1}}^{2}\right] \\
\leq -\alpha_{k}\mu||\nabla F(\mathbf{w}_{k})||_{\mathbf{M}^{-1}}^{2} + \frac{1}{2}\alpha_{k}^{2}\hat{L}\left(K_{G}||\nabla F(\mathbf{w}_{k})||_{\mathbf{M}^{-1}}^{2} + K\right) \\
\leq -\left(\mu - \frac{1}{2}\alpha_{k}\hat{L}K_{G}\right)\alpha_{k}||\nabla F(\mathbf{w}_{k})||_{\mathbf{M}^{-1}}^{2} + \frac{1}{2}\alpha_{k}^{2}\hat{L}K$$

Hence, we have the desired inequalities.

The final lemma necessary is as follows.

Lemma 12. Under assumptions 1, 2, and 3 (with F_* being the minimum of F), suppose Eq. 2 is run with a learning rate sequence such that for all $k \in \mathbb{N}$, assume $\alpha_k \leq \frac{\mu}{\hat{L}K_G}$. (Note that α_k could be constant for all $k \in \mathbb{N}$). Then the following inequality holds

(20)
$$\mathbb{E}[F(\mathbf{w}_{k+1}) - F_*] \le (1 - \alpha_k \hat{c}\mu) \mathbb{E}[F(\mathbf{w}_k) - F_*] + \frac{1}{2} \alpha_k^2 \hat{L} K$$

Proof. Given the assumptions and using Lemma 11, we have $\mathbb{E}_{\boldsymbol{\xi}_k}[F(\mathbf{w}_{k+1})] - F(\mathbf{w}_k) \leq -\hat{c}\alpha_k\mu(F(\mathbf{w}_k) - F_*) + \frac{1}{2}\alpha_k^2\hat{L}K$. Subtract F_* from both sides and take the total expectation. We denote this total expectation as $\mathbb{E}[\cdot]$, which represents the expected value taken with respect to all random variables. That is, $\mathbb{E}[F(\mathbf{w}_k)] = \mathbb{E}_{\boldsymbol{\xi}_1}\mathbb{E}_{\boldsymbol{\xi}_2}\dots\mathbb{E}_{\boldsymbol{\xi}_{k-1}}[F(\mathbf{w}_k)]$.

$$\mathbb{E}[\mathbb{E}_{\boldsymbol{\xi}_{k}}[F(\mathbf{w}_{k+1})] - F(\mathbf{w}_{k}) - F_{*}] \leq \mathbb{E}\left[-\hat{c}\alpha_{k}\mu(F(\mathbf{w}_{k}) - F_{*}) + \frac{1}{2}\alpha_{k}^{2}\hat{L}K - F_{*}\right]$$

$$\mathbb{E}[\mathbb{E}_{\boldsymbol{\xi}_{k}}[F(\mathbf{w}_{k+1})] - F_{*}] \leq \mathbb{E}\left[-\hat{c}\alpha_{k}\mu(F(\mathbf{w}_{k}) - F_{*}) - F(\mathbf{w}_{k}) - F_{*}\right] + \frac{1}{2}\alpha_{k}^{2}\hat{L}K$$

$$\leq \mathbb{E}\left[-\hat{c}\alpha_{k}\mu F(\mathbf{w}_{k}) + \hat{c}\alpha_{k}\mu F_{*} + F(\mathbf{w}_{k}) - F_{*}\right] + \frac{1}{2}\alpha_{k}^{2}\hat{L}K$$

$$\leq (1 - \hat{c}\alpha_{k}\mu)\mathbb{E}[F(\mathbf{w}_{k}) - F_{*}] + \frac{1}{2}\alpha_{k}^{2}\hat{L}K$$

which is our desired inequality (20).

Proofs of main theorems

Proof of Theorem 2 Proof. Using Lemma 11, we have for all $k \in \mathbb{N}$:

$$\begin{split} \mathbb{E}_{\boldsymbol{\xi}_{k}}[F(\mathbf{w}_{k+1})] - F(\mathbf{w}_{k}) &\leq -(\mu - \frac{1}{2}\overline{\alpha}\hat{L}K_{G})\overline{\alpha}||\nabla F(\mathbf{w}_{k})||_{\mathbf{M}^{-1}}^{2} + \frac{1}{2}\overline{\alpha}^{2}\hat{L}K \\ &\leq -\left(\mu - \frac{1}{2}\left(\frac{\mu}{\hat{L}K_{G}}\right)\hat{L}K_{G}\right)\overline{\alpha}||\nabla F(\mathbf{w}_{k})||_{\mathbf{M}^{-1}}^{2} + \frac{1}{2}\overline{\alpha}^{2}\hat{L}K \\ &= -\frac{1}{2}\overline{\alpha}\mu||\nabla F(\mathbf{w}_{k})||_{\mathbf{M}^{-1}}^{2} + \frac{1}{2}\overline{\alpha}^{2}\hat{L}K \\ &\leq -\frac{1}{2}\overline{\alpha}\mu[2\hat{c}(F(\mathbf{w}_{k}) - F(\mathbf{w}_{*}))] + \frac{1}{2}\overline{\alpha}^{2}\hat{L}K \\ &\leq -\overline{\alpha}\hat{c}\mu(F(\mathbf{w}_{k}) - F_{*}) + \frac{1}{2}\overline{\alpha}^{2}\hat{L}K \end{split}$$

Now, subtract the constant $\frac{\overline{\alpha}\hat{L}K}{2\hat{c}\mu}$ from both sides of inequality (Eq. 20)

(21)
$$\mathbb{E}[F(\mathbf{w}_{k+1}) - F_*] - \frac{\overline{\alpha}\hat{L}K}{2\hat{c}\mu} \le (1 - \overline{\alpha}\hat{c}\mu)\mathbb{E}[F(\mathbf{w}_k) - F_*] + \frac{1}{2}\overline{\alpha}\hat{L}K - \frac{\overline{\alpha}\hat{L}K}{2\hat{c}\mu}$$

(22)
$$= (1 - \overline{\alpha}\hat{c}\mu) \left(\mathbb{E}[F(\mathbf{w}_k) - F_*] - \frac{\overline{\alpha}\hat{L}K}{2\hat{c}\mu} \right)$$

We must now notice the following chain of inequalities.

$$0 < \overline{\alpha}\hat{c}\mu \le \frac{\hat{c}\mu^2}{\hat{L}K_G}$$

This inequality holds by the theorem assumption that $0 < \overline{\alpha} \le \frac{\mu}{\hat{L}K_G}$.

$$\frac{\hat{c}\mu^2}{\hat{L}K_G} \le \frac{\hat{c}\mu^2}{\hat{L}\mu^2} = \frac{\hat{c}}{\hat{L}}$$

This inequality holds by (16) from Assumption 3.

Now, note that since $\hat{c} \leq \hat{L}$, it follows that $\frac{\hat{c}}{\hat{L}} \leq 1$. The result thus follows by applying 11 repeatedly through iteration $k \in \mathbb{N}$.

Corollary 13. If $g(\mathbf{w}_k, \boldsymbol{\xi}_k)$ is an unbiased estimate of $\nabla F(w_k)$, and the variance of $g(\mathbf{w}_k, \boldsymbol{\xi}_k)$ is bounded by a constant K independent of $\nabla F(\mathbf{w}_k)$, Then for a fixed learning rate bounded by $\frac{K_G}{\hat{L}K_G}$, $\mathbb{E}[F(\mathbf{w}_k) - F_*]$ decreases to below $\frac{\bar{\alpha}\hat{L}K}{2\hat{c}\mu}$ at the rate of $\frac{\hat{c}}{\hat{L}}$.

Proof of Theorem 3 Proof. Since the learning rates are diminishing and by the theorem statement, we have $\alpha_k \hat{L}K_G \leq \alpha_1 \hat{L}K_G \leq \mu$ for all $k \in \mathbb{N}$. By Lemma 11 and Assumption 3,

$$\mathbb{E}_{\boldsymbol{\xi}_{k}}[F(\mathbf{w}_{k+1})] - F(\mathbf{w}_{k}) \leq -(\mu - \frac{1}{2}\alpha_{k}\hat{L}K_{G})\alpha_{k}||\nabla F(\mathbf{w}_{k})||_{\mathbf{M}^{-1}}^{2} + \frac{1}{2}\alpha_{k}^{2}\hat{L}K$$

$$\leq -(\mu - \frac{1}{2}\mu)\alpha_{k}||\nabla F(\mathbf{w}_{k})||_{\mathbf{M}^{-1}}^{2} + \frac{1}{2}\alpha_{k}^{2}\hat{L}K$$

$$\leq -\alpha_{k}\mu\hat{c}(F(\mathbf{w}_{k}) - F_{*}) + \frac{1}{2}\alpha_{k}^{2}\hat{L}K$$

By Lemma 12, using (20), we have

$$\mathbb{E}[F(\mathbf{w}_{k+1}) - F_*] \le (1 - \alpha_k \hat{c}\mu) \mathbb{E}[F(\mathbf{w}_k) - F_*] + \frac{1}{2} \alpha_k^2 \hat{L} K$$

Now, we prove the convergence result via induction. Consider the base case, k=1. Since $\nu \geq (\gamma+1)(F(\mathbf{w}_1)-F_*)$ and $\nu \geq \frac{\beta^2 \hat{L} K}{2(\beta \hat{c} \mu-1)}$, it follows that $\mathbb{E}[F(\mathbf{w}_1)-F_*] \leq \frac{\nu}{\gamma+1}$. Now, we assume that (8) holds for some $k \geq 1$. Thus

$$\mathbb{E}[F(\mathbf{w}_{k+1}) - F_*] \leq (1 - \alpha_k \hat{c}\mu) \mathbb{E}[F(\mathbf{w}_k) - F_*] + \frac{1}{2} \alpha_k^2 \hat{L} K$$

$$\leq (1 - \alpha_k \hat{c}\mu) \frac{\nu}{\gamma + k} + \frac{1}{2} \alpha_k^2 \hat{L} K$$

$$= \left(1 - \frac{\beta}{\gamma + k} \hat{c}\mu\right) \frac{\nu}{\gamma + k} + \frac{1}{2} \left(\frac{\beta}{\gamma + k}\right)^2 \hat{L} K$$

$$= \left(1 - \frac{\beta \hat{c}\mu}{\tilde{k}}\right) \frac{\nu}{\tilde{k}} + \frac{\beta^2 \hat{L} K}{2\tilde{k}^2}$$

$$= \left(\frac{\tilde{k} - 1}{\tilde{k}^2}\right) \nu - \left(\frac{\beta \hat{c}\mu - 1}{\tilde{k}^2}\right) \nu + \frac{\beta^2 \hat{L} K}{2\tilde{k}^2}$$

where $\tilde{k} := \gamma + k$. Note that $\left(\frac{\beta \hat{c}\mu - 1}{\tilde{k}^2}\right)\nu - \frac{\beta^2 \hat{L}K}{2\tilde{k}^2} \ge 0$ since $\nu \ge \frac{\beta^2 \hat{L}K}{2(\beta \hat{c}\mu - 1)}$. Thus,

$$\mathbb{E}[F(\mathbf{w}_{k+1}) - F_*] \le \left(\frac{\tilde{k} - 1}{\tilde{k}^2}\right) \nu - \left(\frac{\beta \hat{c}\mu - 1}{\tilde{k}^2}\right) \nu + \frac{\beta \hat{L}K}{2\tilde{k}^2} \le \frac{\nu}{\tilde{k} + 1}$$

where (†) follows since $\tilde{k}^2 \geq (\tilde{k}+1)(\tilde{k}-1)$.

Proof of Theorem 4 Proof. Let $\mathcal{F}_k := \sigma(\boldsymbol{\xi}_1, \dots, \boldsymbol{\xi}_{k-1})$ and fix $\alpha_k := \overline{\alpha}$. Define the stopped iterates $\widetilde{\mathbf{w}}_k := \mathbf{w}_{k \wedge \tau}$ with

$$\tau := \inf\{k \ge 1 : \mathbf{w}_k \notin \mathcal{N}_r\}, \qquad g_k := g(\mathbf{w}_k, \boldsymbol{\xi}_k).$$

Then

$$\widetilde{\mathbf{w}}_{k+1} = \widetilde{\mathbf{w}}_k - \overline{\alpha} \mathbf{1}_{\{k < \tau\}} \mathbf{M}^{-1} g_k,$$

and if $k \geq \tau$ then $\widetilde{\mathbf{w}}_{k+1} = \widetilde{\mathbf{w}}_k$.

For $k < \tau$ we have $\mathbf{w}_k \in \mathcal{N}_r \subset \mathcal{N}_{r_+} \subset \mathcal{V}$, and by one–step containment $\mathbf{w}_{k+1} \in \mathcal{N}_{r_+} \subset \mathcal{V}$. Since \mathcal{V} is convex, the segment $[\mathbf{w}_k, \mathbf{w}_{k+1}] \subset \mathcal{V}$, so the M–smoothness inequality applies:

$$(23) F(\widetilde{\mathbf{w}}_{k+1}) \leq F(\widetilde{\mathbf{w}}_k) - \overline{\alpha} \mathbf{1}_{\{k < \tau\}} \nabla F(\widetilde{\mathbf{w}}_k)^{\mathsf{T}} \mathbf{M}^{-1} g_k + \frac{\hat{L}}{2} \overline{\alpha}^2 \mathbf{1}_{\{k < \tau\}} \|g_k\|_{\mathbf{M}^{-1}}^2.$$

Taking $\mathbb{E}[\cdot \mid \mathcal{F}_k]$ in (23) and using Assumption 6 together with $\widetilde{\mathbf{w}}_k = \mathbf{w}_k$ on $\{k < \tau\}$ yields

$$\mathbb{E}[F(\widetilde{\mathbf{w}}_{k+1}) \mid \mathcal{F}_k] \leq F(\widetilde{\mathbf{w}}_k) - \overline{\alpha} \, \mu \, \mathbf{1}_{\{k < \tau\}} \|\nabla F(\widetilde{\mathbf{w}}_k)\|_{\mathbf{M}^{-1}}^2 + \frac{\hat{L}}{2} \overline{\alpha}^2 \, \mathbf{1}_{\{k < \tau\}} \left(K_G \|\nabla F(\widetilde{\mathbf{w}}_k)\|_{\mathbf{M}^{-1}}^2 + K \right).$$

Since $\overline{\alpha} \leq \mu/(\hat{L}K_G)$ (when $K_G > 0$), we have $\mu \overline{\alpha} - \frac{\hat{L}}{2} \overline{\alpha}^2 K_G \geq \frac{1}{2} \mu \overline{\alpha}$, and thus

(24)
$$\mathbb{E}[F(\widetilde{\mathbf{w}}_{k+1}) \mid \mathcal{F}_k] \leq F(\widetilde{\mathbf{w}}_k) - \frac{1}{2} \mu \overline{\alpha} \mathbf{1}_{\{k < \tau\}} \|\nabla F(\widetilde{\mathbf{w}}_k)\|_{\mathbf{M}^{-1}}^2 + \frac{\hat{L}}{2} \overline{\alpha}^2 K,$$

where we have used $\mathbf{1}_{\{k < \tau\}} \leq 1$ to relax the K-term.

On the other hand, by Assumption 4, for all k with $\widetilde{\mathbf{w}}_k \in \mathcal{N}_r$,

$$\|\nabla F(\widetilde{\mathbf{w}}_k)\|_{\mathbf{M}^{-1}}^2 \geq 2\hat{\mu}_{\mathrm{PL}}(F(\widetilde{\mathbf{w}}_k) - F_*).$$

Substituting this into (24) and writing

$$\rho := \overline{\alpha} \, \hat{\mu}_{\rm PL} \, \mu, \qquad C := \frac{\overline{\alpha} \, \hat{L} K}{2 \, \hat{\mu}_{\rm PL} \, \mu},$$

we obtain

(25)
$$\mathbb{E}[F(\widetilde{\mathbf{w}}_{k+1}) - F_* \mid \mathcal{F}_k] \le (1 - \rho \mathbf{1}_{\{k < \tau\}}) (F(\widetilde{\mathbf{w}}_k) - F_*) + \rho C.$$

Let $\Omega_{\infty} := \{ \tau = \infty \}$. On Ω_{∞} we have $\mathbf{w}_k \in \mathcal{N}_r$ for all k, so $\widetilde{\mathbf{w}}_k = \mathbf{w}_k$ and $\mathbf{1}_{\{k < \tau\}} \equiv 1$. Restricting (25) to Ω_{∞} gives

$$\mathbb{E}[F(\mathbf{w}_{k+1}) - F_* \mid \mathcal{F}_k, \Omega_{\infty}] \le (1 - \rho) (F(\mathbf{w}_k) - F_*) + \rho C.$$

Setting $x_k := \mathbb{E}[F(\mathbf{w}_k) - F_* \mid \Omega_{\infty}]$ and taking expectations under $\mathbb{P}(\cdot \mid \Omega_{\infty})$ yields

$$x_{k+1} \leq (1-\rho) x_k + \rho C.$$

Since $\rho \in (0,1)$ by $\overline{\alpha} < 1/(\mu \hat{\mu}_{\rm PL})$, iterating this recursion yields

$$x_k \le C + (1-\rho)^{k-1}(x_1-C) = C + (1-\rho)^{k-1}(F(\mathbf{w}_1) - F_* - C),$$

which proves the first claim.

For the stability bound, we return to the stopped process and use (25) without conditioning on Ω_{∞} . Define $Y_k := F(\widetilde{\mathbf{w}}_k) - F_* - C$. Then (25) implies

$$\mathbb{E}[Y_{k+1} \mid \mathcal{F}_k] \leq (1 - \rho \, \mathbf{1}_{\{k < \tau\}}) \, Y_k,$$

so $(Y_{k \wedge \tau})_{k \geq 1}$ is a supermartingale. Optional stopping at time $\tau \wedge k$ gives

$$\mathbb{E}[Y_{\tau \wedge k}] \leq Y_1 = F(\mathbf{w}_1) - F_* - C.$$

On the event $\{\tau \leq k\}$ we have $\mathbf{w}_{\tau} \in \mathcal{N}_{r_{+}} \setminus \mathcal{N}_{r}$, so by QG (Assumption 7) and the fact that $\operatorname{dist}_{\mathbf{M}}(\mathbf{w}_{\tau}, \mathcal{S}) \geq r$,

$$F(\mathbf{w}_{\tau}) - F_* \ge \frac{\alpha_{QG}}{2} r^2$$
, hence $Y_{\tau} = F(\mathbf{w}_{\tau}) - F_* - C \ge \frac{\alpha_{QG}}{2} r^2 - C$.

On $\{\tau > k\}$, we have $\widetilde{\mathbf{w}}_k = \mathbf{w}_k \in \mathcal{N}_r$, so $F(\widetilde{\mathbf{w}}_k) \geq F_*$ and thus $Y_k \geq -C$. Therefore,

$$\mathbb{E}[Y_{\tau \wedge k}] \ge \left(\frac{\alpha_{QG}}{2} r^2\right) \mathbb{P}(\tau \le k) - C.$$

Combining this with $\mathbb{E}[Y_{\tau \wedge k}] \leq F(\mathbf{w}_1) - F_* - C$ yields

$$\mathbb{P}(\tau \le k) \le \frac{F(\mathbf{w}_1) - F_*}{\frac{\alpha_{QG}}{2} r^2}.$$

Letting $k \to \infty$ gives

$$\mathbb{P}(\tau = \infty) \geq 1 - \frac{F(\mathbf{w}_1) - F_*}{\frac{\alpha_{QG}}{2} r^2},$$

which proves the second claim.

Proof of Theorem 5 Proof. Let $\mathcal{F}_k := \sigma(\boldsymbol{\xi}_1, \dots, \boldsymbol{\xi}_{k-1})$ and set $\alpha_k = \beta/(\gamma + k)$. Define the stopped iterates $\widetilde{\mathbf{w}}_k := \mathbf{w}_{k \wedge \tau}$ with

$$\tau := \inf\{k \ge 1 : \mathbf{w}_k \notin \mathcal{N}_r\}, \qquad g_k := g(\mathbf{w}_k, \boldsymbol{\xi}_k).$$

Then a.s.

$$\widetilde{\mathbf{w}}_{k+1} = \widetilde{\mathbf{w}}_k - \alpha_k \, \mathbf{1}_{\{k < \tau\}} \, \mathbf{M}^{-1} g_k,$$

and if $k \geq \tau$ both sides equal $\widetilde{\mathbf{w}}_k$.

By one–step containment and local M–smoothness on a convex neighborhood $\mathcal{V} \supset \mathcal{N}_{r_+}$,

$$F(\widetilde{\mathbf{w}}_{k+1}) \leq F(\widetilde{\mathbf{w}}_k) - \alpha_k \, \mathbf{1}_{\{k < \tau\}} \nabla F(\widetilde{\mathbf{w}}_k)^{\mathsf{T}} \mathbf{M}^{-1} g_k + \frac{\hat{L}}{2} \, \alpha_k^2 \, \mathbf{1}_{\{k < \tau\}} \|g_k\|_{\mathbf{M}^{-1}}^2.$$

Taking $\mathbb{E}[\cdot \mid \mathcal{F}_k]$ and using the local stochastic conditions on \mathcal{N}_r gives

$$\mathbb{E}[F(\widetilde{\mathbf{w}}_{k+1}) \mid \mathcal{F}_k] \leq F(\widetilde{\mathbf{w}}_k) - \alpha_k \, \mu \, \mathbf{1}_{\{k < \tau\}} \|\nabla F(\widetilde{\mathbf{w}}_k)\|_{\mathbf{M}^{-1}}^2 + \frac{\hat{L}}{2} \, \alpha_k^2 \, \mathbf{1}_{\{k < \tau\}} \left(K_G \|\nabla F(\widetilde{\mathbf{w}}_k)\|_{\mathbf{M}^{-1}}^2 + K \right)$$

Since $\alpha_k \leq \alpha_1 \leq \mu/(\hat{L}K_G)$, we have $\mu\alpha_k - \frac{\hat{L}}{2}\alpha_k^2K_G \geq \frac{\mu}{2}\alpha_k$; using local **M**-PL on \mathcal{N}_r , with $S_k := F(\widetilde{\mathbf{w}}_k) - F_*$, $m := \mu\hat{\mu}_{\mathrm{PL}}$, and $c := \hat{L}K/2$,

(26)
$$\mathbb{E}[S_{k+1} \mid \mathcal{F}_k] \leq S_k - m \alpha_k \mathbf{1}_{\{k < \tau\}} S_k + c \alpha_k^2 \mathbf{1}_{\{k < \tau\}}.$$

Let $\Omega_{\infty} := \{ \tau = \infty \}$. Multiply (26) by $\mathbf{1}_{\Omega_{\infty}}$ and take expectations; since $\mathbf{1}_{\Omega_{\infty}} \mathbf{1}_{\{k < \tau\}} = \mathbf{1}_{\Omega_{\infty}}$, $\mathbb{E}[S_{k+1} \mathbf{1}_{\Omega_{\infty}}] \leq \mathbb{E}[(1 - m\alpha_k) S_k \mathbf{1}_{\Omega_{\infty}}] + c \alpha_k^2 \mathbb{E}[\mathbf{1}_{\Omega_{\infty}}]$.

Dividing by $\mathbb{P}(\Omega_{\infty})$ gives

$$x_{k+1} \le \left(1 - \frac{a}{\gamma + k}\right) x_k + \frac{b}{(\gamma + k)^2},$$

where $x_k := \mathbb{E}[S_k \mid \Omega_{\infty}]$, $a := \beta m = \beta \mu \hat{\mu}_{PL}$, and $b := \frac{1}{2}\hat{L}K\beta^2$. Because $\beta > 2/(\mu \hat{\mu}_{PL})$, a > 1, and the standard scalar lemma yields

$$\mathbb{E}[F(\mathbf{w}_k) - F_* \mid \tau = \infty] = x_k \le \frac{\nu}{\gamma + k}, \qquad \nu := \max \left\{ \frac{\beta^2 \hat{L} K}{2(\beta \hat{\mu}_{\mathrm{PL}} \mu - 1)}, \ (\gamma + 1) [F(\mathbf{w}_1) - F_*] \right\}.$$

Set
$$\widetilde{C} := \frac{\widehat{L}K}{2\widehat{\mu}_{\mathrm{BH}}\mu}\alpha_1$$
 and $Y_k := F(\widetilde{\mathbf{w}}_k) - F_* - \widetilde{C}$. From (26) and $\alpha_k \leq \alpha_1$,

$$\mathbb{E}[Y_{k+1} \mid \mathcal{F}_k] \leq Y_k - m \, \alpha_k \, \mathbf{1}_{\{k < \tau\}} \, Y_k + \left(c \, \alpha_k^2 - m \, \alpha_k \, \widetilde{C} \right) \mathbf{1}_{\{k < \tau\}} \leq Y_k,$$

so $(Y_{k \wedge \tau})_{k \geq 1}$ is a supermartingale and $\mathbb{E}[Y_{\tau \wedge k}] \leq Y_1 = F(\mathbf{w}_1) - F_* - \widetilde{C}$. On $\{\tau \leq k\}$, one—step containment and local QG on \mathcal{N}_{r_+} imply $Y_{\tau} \geq \frac{\alpha_{\text{QG}}}{2} r^2 - \widetilde{C}$; on $\{\tau > k\}$, $Y_k \geq -\widetilde{C}$. Therefore,

$$\mathbb{P}(\tau \leq k) \leq \frac{F(\mathbf{w}_1) - F_*}{\frac{\alpha_{\text{QG}}}{2} r^2}, \quad \text{and letting } k \to \infty \text{ yields} \quad \mathbb{P}(\tau = \infty) \geq 1 - \frac{F(\mathbf{w}_1) - F_*}{\frac{\alpha_{\text{QG}}}{2} r^2}.$$

Numerical experiments

Implementation details The algorithms in this paper were implemented in Python using jax (version 0.5.0), flax (version 0.10.0), and optax (version 0.2.4). All timing results reported in Section were measured on a consistent hardware platform running Ubuntu 24.04.2 LTS, equipped with an Intel(R) Core(TM) i7-12700K CPU (8 Performance-cores @ 3.60 GHz and 4 Efficient-cores @ 2.70 GHz), and 64 GB of system memory. All experiments were executed in double precision arithmetic to ensure numerical stability for the challenging SciML problems.

Baseline methods and experimental setting Our experiments evaluated several optimization algorithms to validate our theoretical analysis of preconditioning effects. We implemented vanilla SGD, SGD with momentum ($\beta = 0.9$), and the preconditioned methods using GGN and Hessian approximations. The preconditioned methods employ conjugate gradient to efficiently approximate matrix-vector products with the inverse preconditioner, avoiding the prohibitive cost of explicitly forming and inverting the full matrices. This approach provides a computationally tractable way to incorporate curvature information into the optimization process. For Adam (with $\beta_1 = 0.9$, $\beta_2 = 0.999$) and L-BFGS (with memory size 100 and maximum line search of 100 steps), we utilized the implementations available in the optax library.

Our experimental protocol employed a structured two-phase optimization strategy. Phase I utilized Adam with a learning rate of 0.001 until convergence slowed significantly. This established a common starting point in the optimization landscape and helped navigate past initial high-gradient regions. In Phase II, we transitioned to the respective optimization methods for direct performance comparison. The specific duration of each phase varied by task complexity and is detailed in the respective experimental sections.

We individually optimized learning rates for each method-task combination through grid search, deliberately omitting learning rate schedulers to isolate the inherent convergence properties of each optimizer. For Adam, we searched within the range $\{0.001, 0.0005, 0.0002, 0.0001, \ldots, 0.00001\}$. The preconditioned methods required different learning rate ranges due to their distinct curvature properties: CG-Hessian used $\{1.0, 0.5, \ldots, 0.001\}$, while CG-GGN employed a range of $\{0.1, 0.05, \ldots, 0.0001\}$. This difference reflects our theoretical analysis that effective preconditioning can support larger learning rates when operating near local minima. For vanilla SGD and momentum SGD, we initially explored the same ranges as Adam and expanded to wider intervals when necessary to ensure optimal performance. This methodology ensured a fair comparison by allowing each optimizer to operate at its most effective learning rate for each specific task.

To ensure robust experimental results, we conducted each experiment five times using different random seeds (42 to 46 for Phase I and 43 to 47 for Phase II). This approach accounts for the inherent stochasticity in neural network training processes and allows us to report mean performance metrics. For our timing analysis, we implemented a precise measurement protocol that isolates the computational efficiency of the optimization methods themselves. Specifically, we excluded all data generation and preprocessing overhead, capturing only the cumulative duration of the actual training iterations on identical hardware configurations. This methodology provides an equitable assessment of computational efficiency, particularly important when comparing methods with substantially different per-iteration costs, such as first-order methods versus preconditioned approaches that require conjugate gradient iterations.

Motivating example: multilayer perceptrons Figure 1 was a simple dense MLP with two hidden layers, each with 256 nodes. The full 60,000 piece fashion MNIST dataset was used. Vanilla SGD was used with no momentum and a fixed learning rate of $\alpha_k = 0.001$ and fixed batch size of $|\mathcal{B}| = 256$. The bounds were calculated. To show that this problem was not special, and most other problems have a linear convergence rate in practice, we ran similar experiments while changing network parameters like the number of nodes in the two hidden layers, the learning rate, the batch size, and the dataset.

First by changing the fixed learning rates to $\{0.001, 0.005, 0.01\}$, as illustrated in Fig7, we observe that a linear decay is observed for all of these learning rates. As the learning rate $\bar{\alpha}$ increases, we see an increase of the linear decay constant, since $(1 - \bar{\alpha}\hat{c}\mu)$ will get smaller. However, there is a tradeoff with using larger learning rates, which is the stochastic floor $C := \frac{\bar{\alpha}\hat{L}K}{2\hat{c}\mu}$ is higher, which is illustrated in the number of epochs the SGD has that linear decay.

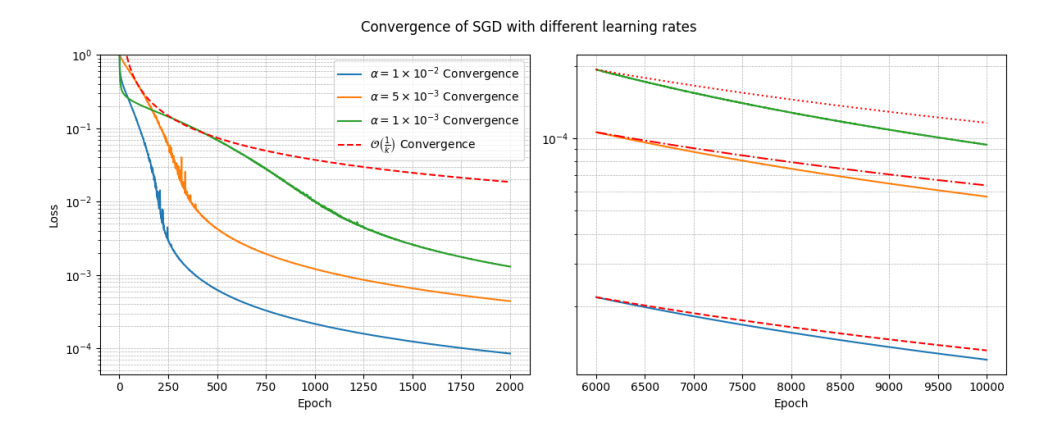


FIGURE 7. Two layer MLP with 256 nodes per layer and batch size 128 trained on the full fashion MNIST dataset. Left: Theoretical $\mathcal{O}(1/k)$ decay (dashed line) versus fixed learning rate SGD convergence. Right: Zoomed in on the asymptotic regime.

This experiment is visualized in Figure 7.

Noisy data regression For the Franke function regression experiment, we used a neural network with two hidden layers of 50 neurons each and ReLU activation functions. We resampled the dataset every epoch, generating 256 points with additive Gaussian noise as described in Appendix and illustrated in the left panel of Figure 8. For the preconditioned methods, we employed 5 conjugate gradient iterations. The right panel of Figure 8 extends our main results by displaying not only the mean performance across 5 independent runs but also the variance bands for each optimization method.

Physics-informed neural networks For solving the Poisson equation with PINNs, we used a neural network with two hidden layers of 50 neurons each and tanh activation functions. We resampled the dataset every epoch, generating 1,000 points within the domain and 200 points on the boundary, as described in Appendix and illustrated in the left panel of Figure 9. For the preconditioned methods, we employed 20 conjugate gradient iterations. The right panel

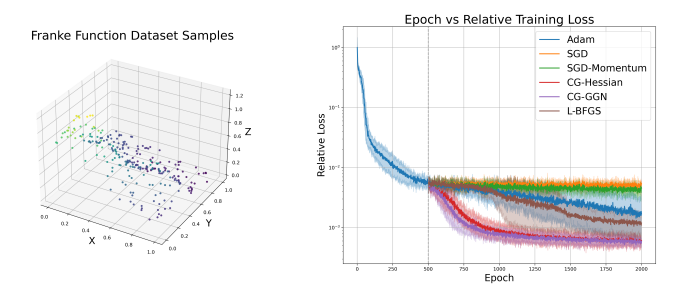


FIGURE 8. Left: Visualization of the Franke function dataset sampling. Right: Franke function regression performance averaged over 5 independent runs. Left: Training loss versus epochs with Phase I transitioning to Phase II at epoch 500 with variance.

of Figure 9 shows that the mean loss trajectory is accompanied by a tight variance envelope across 5 independent runs.

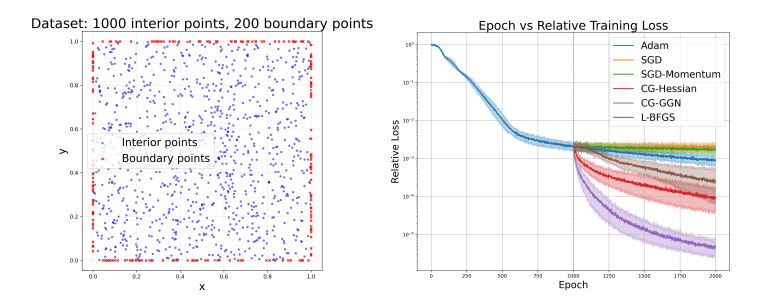


FIGURE 9. Left: Visualization of the sampling strategy for the 2D Poisson equation PINNs. The plot shows the distribution of 1,000 collocation points within the domain (blue) and 200 points along the boundary (red) used for enforcing the PDE and boundary conditions respectively. Right: Poisson equation PINNs performance averaged over 5 independent runs. Training loss versus epochs with Phase I transitioning to Phase II at epoch 1,000 with variance.

Green's function learning For both cases in the Green's function experiments, we used a neural network with five hidden layers of 20 neurons each and tanh activation functions. We resampled the dataset every epoch, generating 1,000 points within the domain, 500 points such that x is close to y, and 200 points on the boundary. For the preconditioned methods, we employed 20 conjugate gradient iterations. Figure 11 extends our main results by displaying not only the mean performance across 5 independent runs but also the variance bands for each optimization method.

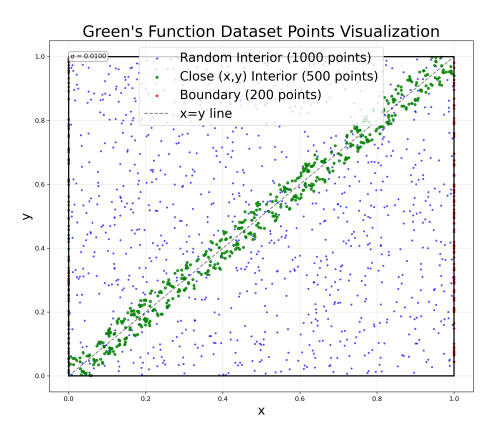


FIGURE 10. Visualization of the sampling strategy for Green's function learning. The plot shows three categories of training points: randomly distributed interior points (blue, 1,000 points), points concentrated near the diagonal where x is close to y (green, 500 points) to capture the near-singularity behavior characteristic of Green's functions, and boundary points (red, 200 points) used to enforce homogeneous Dirichlet boundary conditions.

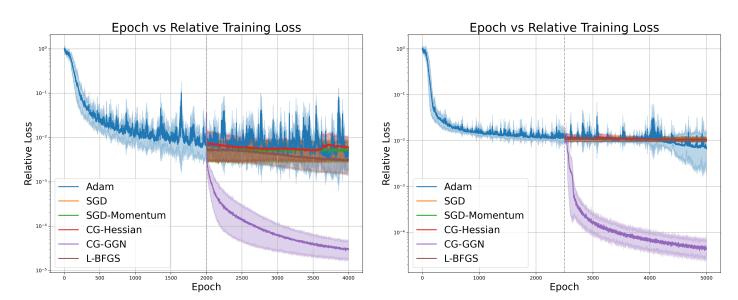


FIGURE 11. Green's function learning performance averaged over 5 independent runs. Left: Training loss versus epochs with Phase I transitioning to Phase II at epoch 2,000 with variance for Laplacian. Right: Training loss versus epochs with Phase I transitioning to Phase II at epoch 2,500 with variance for convection-diffusion.